Nanoscale

Accepted Manuscript

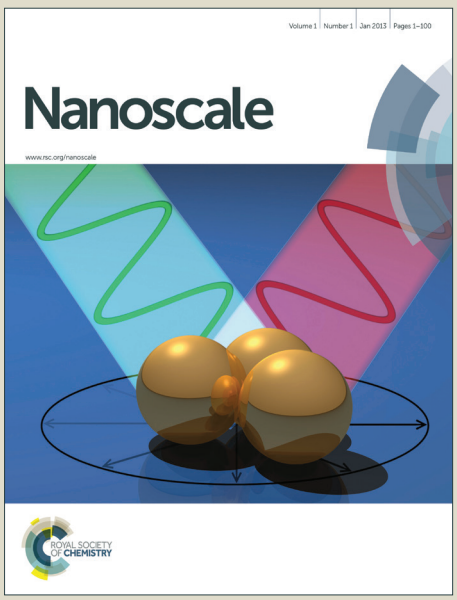

ROYAL SOCIETY OF CHEMISTRY

www.rsc.org/nanoscale

Journal Name

RSCPublishing

ARTICLE

Metal-Organic Framework Composites: From Fundamentals to Applications

Cite this: DOI: 10.1039/xoxx00000x

Shaozhou Li[a*] and Fengwei Huo [b*]

Received ooth January 2012,
Accepted ooth January 2012

DOI: 10.1039/xoxx00000x

www.rsc.org/

Metal-organic frameworks (MOFs) are a class of crystallized porous polymeric materials consisting of metal ions or clusters linked together by organic bridging ligands. Due to their permanent porosity, rich surface chemistries and tuneable pore sizes, MOFs have emerged as one kind of important porous solid and attracted intensive interests in catalysis, gas adsorption, separation and storage over the past two decades. Compared with pure MOFs, the combination of MOFs with functional species or matrix materials not only shows enhanced properties, but also broadens the applications of MOFs to new fields such as bio-imaging, drug delivery and electrical catalysis owing to the interactions of the functional species/matrix with the MOF structures. Although the synthesis, chemical modifications and potential applications of MOFs have been reviewed previously, there is increasing awareness on the synthesis and applications of their composites which have rarely been reviewed. This review aims to fill this gap and discuss the fabrication, properties, and applications of MOF composites. The remaining challenges and future opportunities in this field, in terms of processing techniques, maximizing composite properties, and prospects for applications, have also been indicated.

1. Introduction

Metal-organic frameworks (MOFs), also known as porous coordination polymers (PCPs), are a class of crystallized porous polymeric materials formed by the coordination of metal ions/clusters and organic bridging ligands. Although the synthesis of coordination polymers with microporous structures such as Prussian blue can be traced even back to the 18th century, [1] the systematic studies of MOF synthesis and their applications only started about two decades ago. The pioneer work has been done by Robson, [2, 3] Moore, [4, 5] Yaghi, [6] and Zaworotko [7] in early 1990s. From then on, attracted by the vision that such materials can be incorporated with the designed structural, magnetic, electrical, optical, and catalytic properties through choosing appropriate metal ions and organic ligands, many scientists started to join this young but dynamic field. With their effort, many synthetic strategies have been developed to form the MOFs with different crystal structures, pore sizes and surface chemistries.[8, 9]

Compared with other porous materials such as zeolites, active carbon and mesoporous silica, MOFs show a better chemical tailorability owing to their diversified functional groups on the frameworks. This rewards MOFs with the applications beyond traditional areas of porous materials (such as molecule storage, [10, 11] separation, [12, 13] and catalysis[14, 15]) which mainly utilize the pore structures of materials.[16-18] However, the fragileness of the functional groups in ligands of MOFs greatly restricts the development and application of functional MOFs. For the applications such as sensing and catalysis, *robust* MOFs are required which excludes many MOFs formed by the room temperature synthetic strategies as the MOFs synthesized under low temperature are rarely highly thermally or chemically stable.[19] To form sturdy MOFs, elevated temperatures, solvothermal reactions or the microwave irradiations are often employed to activate the coordination reactions. These on the other hand degrade the active functional groups on the ligands and thus restrict the functionalities of the MOFs synthesized. Some alternative approaches have been developed to circumvent these issues and post-synthetic method is one popular strategy among them. Through chemical modifications of the organic linkers in MOFs with designed functional groups, this method can introduce functionalities into the MOFs preformed.[20, 21]

The study of MOFs was originally carried out by chemists from both the fields of coordination and solid-state/zeolite chemistry. Recently, MOFs also attract the growing attentions of material scientists. Like the method of post-synthetic modification of MOFs via a series of chemical reactions was adopted by chemists to introduce the functionalities, material scientists learn from the development of composite materials and tend to impart functionalities into MOFs by the integration of functional species such as organic dyes, small bio-molecules, NPs, NWs, nanofibers and polymers through the formation of

composites.[22-23] MOF composites can be made either ① by growing or depositing of MOFs on a two-dimensional planar or curved substrate to form the thin films, or ② by incorporating MOFs with other components to form mixed structures. The preparations and applications of MOF thin films grown on different substrates have been fully reviewed by Bradshaw and Fischer, separately.[24, 25] Therefore, this review will focus on the second case and try to provide a broad overview of the MOF composite materials that have this far been reported. Strategies employed to synthesize MOF composites according to their formation process were introduced first and the potential applications and adopted application-specific configurations of MOF composites were discussed as follows. Finally, the current challenges and future opportunities of MOF composites, in terms of processing techniques, maximizing composite properties, and prospects for applications were provided.

2. The formation of MOF composites

Composite is a solid material composing of two or more substances which retain their own identity while contributing desirable properties to the whole system. Usually, there is at least one substance dominating the material which is denoted as the matrix. Therefore, the MOF composites formed were described as A/B in this paper in which A stands for the functional species and B denotes the matrix materials as adopted by Stock and Biswas.[19] Such notation has also been adopted by the nomenclature of the traditional composite materials.[26] The physicalfragility of MOFs has greatly limited their fabrication processibility. [27] Thus, MOF/A composites in which the MOF crystals were embedded into one continuous, flexible matrix have been produced for the applications such as small molecule separation, purification and catalysis. The matrices in such structures not only allow the reuse and recover of the MOFs, but also enhance the formability of MOF materials. Apart from functional species, MOFs themselves can also serve as matrices for the applications such as heterogeneous catalysis and drug delivery which correlating to the functionalities stemming from both the MOFs and the active species having been imparted. In these applications, MOFs are the stabilizing matrix materials to provide confined spaces for the functional species. The unique structures of MOFs not only restrict the possible diffusions and aggregations of species loaded in the MOFs, but also can change the reaction pathways taking placed, thus leading to new catalytic properties.

2.1 MOFs as functional species

The applications of MOFs for molecule storage, separation and catalysis are limited by their poor processability. To circumvent this difficulty, researchers start to investigate the incorporation of MOF crystals into polymer matrices. Polymers have the advantage of good mechanical, thermal and chemical stability. Moreover, the good formability of polymers also eases the fabrications of their composites. Apart from polymers, inorganic materials like porous silica and porous alumina have also been used as the matrices. Based on the processes involved, the formation of MOF/matrix composites can be categorized as follows (Figure 1):

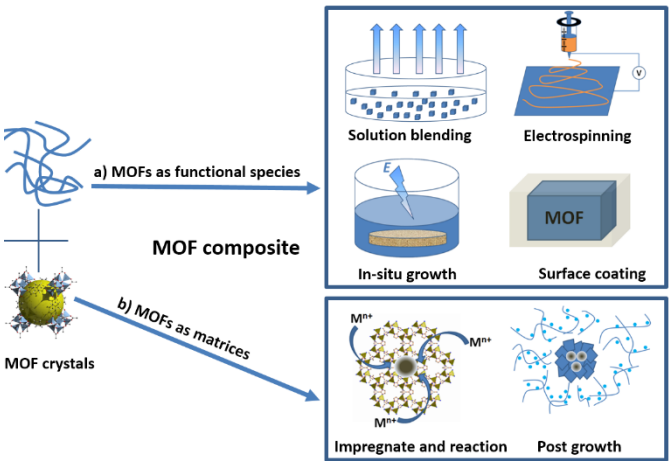

Figure 1. Overview of the MOF composites and their correlated synthesis methods. The composites are categorized as (a) MOFs as functional species, and (b) MOFs as matrix materials.

2.1.1 Formation of MOF composites by solution blending method

The solution blending method is briefly described as this. Mechanical stirring or sonication was applied to the mixture of polymers and the functional species to enhance homogeneity of the incorporated materials in solution before the solvent is vaporized to leave a polymer-based composite. As many polymers can dissolve into liquid solvents, this method has been widely used in the synthesis of polymer-based composites.[28] Flexible MOF/polymer membranes such as HKUST-1/PMMA,[29] ZIF-8/PI,[30] ZIF-90/matrimid, [31] MOF-5/matrimid, [32] HKUST-1/matrimid, [33] Cu-BPY-HFS/matrimid, [34] CuTPA/PVA [35] and ZIF-8/PSU[36] have been produced by this method. The ease of mass production makes these MOF/polymer membranes highly in demand for industrial applications. However, the variation of MOF lattice resulted from the host-guest interactions of MOF structures when solvents removal leads to a weak adhesion between polymers and MOF particles. Moreover, the MOF/polymer membranes formed are often highly defective with uncontrollable voids inside. These issues are undesirable to the membranes used for gas separation and liquid filtration. To improve the compatibility between polymer matrices and MOF particles, *N*-methyl-*N*-(trimethylsilyl)-trifluoroaceamide was used as the silyating agent to modify the surface of MOF particles (HKUST-1, MIL-47, MIL-53 and ZIF-8) before they were incorporated into PDMS.[37] The gas diffusion properties of the membranes formed were studied and an improvement in the gas transport was shown in these MOF/PDMS composite membranes.

2.1.2 Formation of MOF composites by electrospinning

As one technique to produce fibre structures in polymer engineering, electrospinning has also been employed to the

synthesis of MOF/polymer composites. This process can be simply described as follows. A high voltage is applied to a liquid droplet to make it charged, the high cohesion of molecule to liquid leads to the formation of a charged liquid jet and the fast vaporization of solvent during the liquid jet flight results in the formation of fibre composites. This technique allows for an easy generation of fibre composites from a wide variety of MOF/polymer combinations. Moreover, the diameters of fibres and the MOF loadings also can be tuned by varying the polymer concentration and polymer to MOF ratio in the spun mixtures. ZIF-8/PVP, [38] HKUST-1/PS, [39] ZIF-8/PS and MIL-101(Fe)/PS [40] fibrous composites have been produced by this method. With a combination of the facile electrospinning technique and the diversified functionalities of MOFs, the MOF/polymer composite fibres not only show many applications in the fields of gas separation but also can be potentially used for personal protective systems to remove the toxic gases in the environment.[39]

2.1.3 In-situ growth of MOFs in the matrices

In-situ growth is another widely used method to form MOF composite materials. The matrices were immersed into the solution containing MOF precursors and then heated to designed temperature to induce the growth of MOFs on the matrices internal/external surface which yields the formation of MOF composites. Porous metal oxide spheres and porous polymer membranes have been used to synthesis MOF composites by this method.

Silica and alumina microspheres are the widely used matrices for in-situ growth of MOF composites. By solvothermal reaction of HKUST-1 precursor solution in the presence of silica microspheres, HKUST-1 particles were formed and attached firmly on the silica spheres with adjustable porosity.[41, 42] The SIM-1/alumina spheres formed by *in-situ* growth of SIM-1 (a substituted imidazolate-based MOF) onto α or γ-alumina beads under mild heating conditions was reported by S. Aguado *et al.* (Figure 2a).[43] Interestingly, the SIM-1 crystals cover on the α-alumina bead to form a core-shell type structure while the majority of the MOF crystals resides within the cavities of the support when γ-alumina was used. The latter structure is particularly attractive for catalysis applications owing to its good mechanical strength and attrition resistance.

The *in-situ* growth method shows its advantage in palliating the low surface area of MOF composites resulted from the blockage of the MOF pore aperture by polymer chains which is one key issue of the solution blending and electrospinning processes. For example, A MOF/polymer foam was prepared by direct synthesis of UiO-66 over the PU foam template.[44] The composited foam not only maintains the macrostructure and flexibility of PU foam, but also exhibits the micro-porosity, high surface area, and adsorption properties of UiO-66. Through the *in-situ* growth of MOF crystals, HKUST-1 and ZIF-8 on PSU based porous asymmetric ultrafiltration membranes have also been synthesized.[45] Apart from foams and membranes, macro-beads of MOF composites (Co-CPO-27/PAM and HKUST-1/PAM) have also been synthesized by the solvothermal reaction of PAM beads in MOF precursor solutions or via loading the metal ions into the pre-swelled PAM beads, immersing the beads into the ligand solutions and following with solvothermal reaction (Figure 2b).[46] By a step-by-step impregnation and crystallization process, monolithic HCM has also been used as the matrix in which HKUST-1 crystals were *in situ* synthesized to form HKUST-1/HCM composite (Figure 2c).[47]

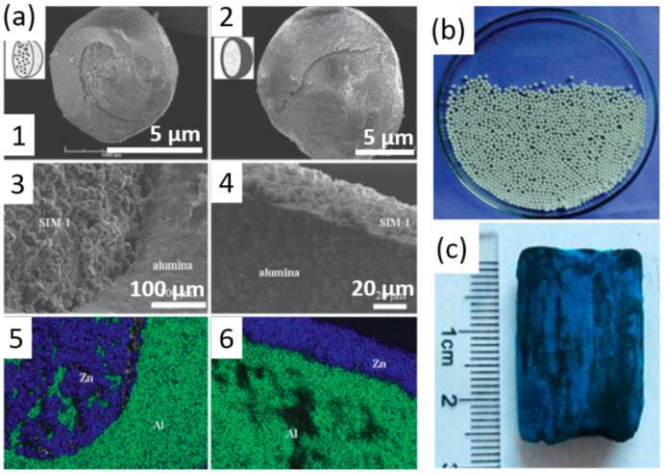

Figure 2. Growth of MOFs in the matrices. (a) SIM-1 supported on γ-alumina and α-alumina beads. (1-2) SEM images of the beads and view of the cross-section. (3-4) SEM image and (5-6) EDS mapping of the core and surface. (b) Digital image of HKUST-1/PAM beads. (c) Digital image of HKUST-1/HCM. Reproduced with permission.[43, 46, 47]

2.1.4 Surface coating with silica or polymers

MOFs can be used for bio-applications such as the bio-imaging and drug delivery. Due to the cytotoxicity and the intrinsic instability of many MOFs under physiological conditions, the MOFs as-synthesized are typically further coated with thin silica or bio-polymer shells to optimize their *in vivo* performance. [17, 48] The silica/polymer coating also used on controlling the release of loaded drugs in MOF cavities during drug delivery.[48] Moreover, these shells also are platforms for surface modifications to both improve the water dispersity of MOFs and add the affinity of MOFs to the molecules to target specific cells or tissues, thus provide the MOF composites with many potential advantages over their pristine counterparts. A silica layer is usually prepared by the slow hydrolysis of TEOS on MOF surface under acidic conditions. By applying this process, Rieter *et al.* have covered the MOF NPs made of a cisplatin derivative and Tb^{3+} ions with a silica shell of around 7 nm.[49] Liu and co-workers have reported the stabilization of phosphorescent ruthenium MOF [Ru-{5,5'-$(CO2H)_2$-bpy}$(bpy)_2$]$(PF_6)_2$([L-H_2]$(PF_6)_2$) with amorphous silica shells.[50] The targeting efficiency of this MOF composite was further improved by a surface coating of PEG and PEG–anisamide (AA). Taylor *et al.* synthesized two Mn-MOFs: Mn(1,4-BDC)$(H_2O)_2$ and $Mn_3(BTC)_2(H_2O)_6$, which were then coated with thin silica shells and subsequently functionalised with a

cyclic peptide c(RGDfK) and a fluorescence dye-Rhodamine B for the target-specific imaging applications.[51]

2.1.5 Other methods

Kaskel *et al.* have demonstrated the incorporation of HKUST-1 particles into polyHIPEs by a three-step synthetic route: [52] ① synthesis of the macroporous polymeric support based on 4-vinylbenzyl chloride cross-linked with divinylbenzene; ② hydrophilization of the polyHIPE by introducing hydroxyl groups into the material; and ③ impregnation with precursor solution and hydrothermal synthesis of HKUST-1 within the interconnected voids of the macroporous monolith. As the polyHIPE composite enclosing MOF crystals can be synthesized with user-defined geometry, this synthetic technique would enhance the workability of the MOF composites produced.

2.2 MOFs as matrix materials

As the matrix materials in composites, MOFs show many unique properties compared with other porous solids: ① The nanometre scaled cavities of MOFs can be accessed by the reactants from exterior and thus allow the direct reaction and formation of active species inside the frameworks, ② The internal surfaces of MOFs are chemically tuneable to optimize the molecule adsorption/binding and chemical reactions, and 3) The designed pore matrices make MOFs excellent sieving materials.

2.2.1 Impregnation of MOFs with functional species

MOFs can be impregnated with precursors through a diffusion/deposition process owing to their accessible pores to metal ions and small molecules. The procedure usually consists of two steps:① MOF solids were immersed into the solution containing the precursors for impregnation, and ② the adsorbed precursors either were the final active species or further reacted (by reduction, decomposition or other chemical pathways) to form new functional phase inside the MOF matrices. MOFs provide a confined space to limit the growth of these functional species and impede their agglomeration. Therefore, highly stable MOFs are often required as a sequential of reactions may be necessary before the formation of final MOF composites.

To impregnate the precursors into MOFs under solvent conditions, three loading strategies, namely direct adsorption, incipient wetness and ion exchange, have been employed. The process of direct adsorption can be described as this. MOF powders were immersed into the solution containing metal ions without considering the stoichiometry of MOFs and metal ions. Metal NPs usually grow indiscriminately inside the MOF cavities and on the MOF outer surface in this approach due to the out-diffusion of precursors during their reduction. Therefore, an incipient wetness infiltration method has been developed to control the spatial distributions of the NPs inside MOFs. Incipient wetness infiltration once was a commonly used technique for the synthesis of heterogeneous catalysts. Typically, the metal precursor is dissolved in a solution which is added to a catalyst support containing the same pore volume as the volume of the solution that was added. The capillary action draws the solution into the pores and solution added in excess of the support pore volume causes the solution transport to change from a capillary action process to a diffusion process, which is much slower. The product can then be calcined to remove the volatile components and leave the metal catalysts deposited. This method has been employed to the synthesis of Pd NP/MOF-5, [53] Pd NP/MIL-101 [54, 55] and Pt NP/MIL-101 composites. [56] To further inhibit the growth and aggregation of NPs on the external surface of MOFs, double solvents have been used for the precursor loading by Xu's group (Figure 3a).[56, 57] Both a hydrophilic solvent (water, containing the metal precursor with a volume set equal to or less than the pore volume of the adsorbent) and a hydrophobic solvent (hexane, suspending the adsorbent and facilitating the impregnation process) were used. Through this method, Pt NPs (size 1.2-3 nm) [56] and AuNi NPs (size 2-5 nm) have been successfully incorporated into MIL-101(Figure 3b).[57] Ion exchange is another loading method (Figure 3c) which is mainly used in the synthesis of Pd NP/MOF composites. The complexes of $PdCl_4^{2-}$-MIL-NH_3^+ were formed by mixing MIL serials MOFs (such as MIL-53(Al), MIL-101(Cr) and MIL-53(Al)-NH_2,which contain or have post-functionalised with amine group) with the solution containing $PdCl_4^{2-}$.The mixture was then reduced by $NaBH_4$ to yield Pd NP/MOF composites.[58-60] Due to the well dispersion of Pd NPs in the composites formed and the high chemical stability of MIL-MOF structures, these materials show high chemical activity in the catalytic reactions.[6]

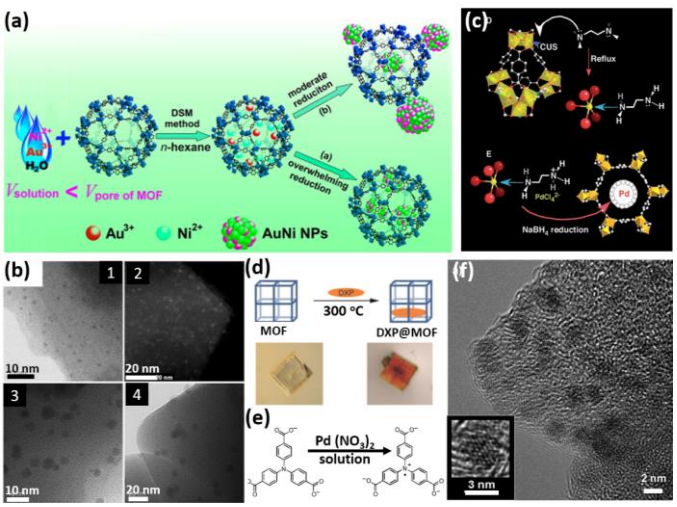

Figure 3. Overview the strategies of forming MOF composites by the impregnation of functional species. (a) Schematic representation of formation metal NP/MOF composites by a double-solvent method. (b) TEM images of the obtained composites of AuNi NP/MIL-101 reduced by different amount of $NaBH_4$. (c) Schematic illustration of the ion exchange method to form Pd NP/MOFs with amine groups. (d) DXP/MOF composite formed by the vapour deposition. (e) and (f) The scheme of Pd NPs formed in MOF SNU-3 by auto-redox and the TEM image of obtained Pd NPs/SNU-3, (f) T Reproduced with permission. [57, 60, 62, 68]

Without further treatments, cluster/MOF and molecule/MOF composites are the products usually formed after the impregnation process. For example, the large mesoporous cage (34 Å) and microporous window (16 Å) of MIL-101(Cr) allows for easy loading of POM clusters, a class of solid-acid catalysts for many acid-catalysed organic transformations and industrial applications, within their pores through liquid filtration.[61] Other clusters such as the highly emissive perylene derivative DXP and the iridium complex, FIrpic have also been incorporated into MOF-5, MOF-177, UMCM-1 and MIL-53(Al) by vapour deposition and a loading rate of 1.4 wt.% for DXP/MOF-5 and 8 wt.% for DXP/UMCM-1 was reported (Figure 3d).[62]

In most of cases, however, the employment of additional chemical treatments such as hydrolysis or chemical reduction are necessary to convert the impregnated precursors into final functional species. $(ZnO)_2$/MOF-5 composite has been synthesized by the vapour deposition of Zn-organometallic precursor in MOF-5 following with a mild hydrolysis/oxidation process.[63] ZnO NP/MOF-5 and TiO_2 NP/MOF-5 were synthesized through the dry oxidation of loaded metal compound precursors such as $ZnEt_2$ or $Ti\{OCH(CH_3)_2\}_4$ in MOF-5 crystals, into their metal oxides, respectively.[64, 65] Metal nitride NPs embedded inside MOFs have also been formed through a similar chemical pathway.[66] A GaN NP/ZIF-8 composite was synthesized by the loading of ZIF-8 with $[(CH_3)_3NGaH_3]$ via vapour deposition which yields $(H_2GaNH_2)_3$/ZIF-8 through ammonia treatment and the intermediate eventually gave the GaN NPs/ZIF-8 composite through further annealing.

Chemical reduction happens in the procedure of converting metal ions impregnated inside MOFs into metal NPs. The reduction can be carried out by MOFs themselves or with the assistance of external stimuli such as reducing agents, solar light, UV and even microwave irradiation. Auto-redox takes place when MOFs with redox sites, such as reductive functional groups on the ligands or metal nodes with low oxidation potential, were used. The idea of synthesizing metal nanostructures encapsulated via redox sites in the porous materials is not totally new. Kim and co-workers have demonstrated the synthesis of single-crystalline Ag NWs of 0.4 nm diameter with CHQ NT as the template.[67] The Ag^+ ions in CHQ were reduced to Ag^0 by hydroxyl groups on inner surfaces of CHQ and the *Ag* atoms then packed along the hydroquinone channel to form Ag NWs. Although some MOFs used for the auto-redox of metal ions show more rigid structures compared with CHQ, it is interesting to note that the metal nanostructures resulted in auto-redox MOFs are not defined by the MOF channels like in CHQ and NPs with average diameters much larger than the MOF pores usually forms.

$[Zn_3(ntb)_2(EtOH)_2]$•4EtOH (denoted as SNU-3) synthesized by Suh's group has been used to reduce Pd ions into NPs.[68] Pd NPs with the size of 3-4 nm were formed inside the channels of SNU-3 owing to the redox of Pd^{2+} by 4, 4', 4''-nitrilotrisbenzoate (ntb^{3-}) (Figure 3e-f) and the doping amount of Pd NPs in composites can be tuned through varying the immersing time of SNU-3 in $Pd(NO_3)_2$ solution. *Rb*-CD-MOF and *Cs*-CD-MOF (CD = γ-cyclodextrin) containing cyclodextrin and OH^- counter ions, have also been used to form the metal NP/MOF composites through auto-redox reactions.[69] After immersing the CD MOFs into $AgNO_3$ or $HAuCl_4$ solution separately, Ag NPs (~2 nm) and Au NPs (3-4 nm) were formed inside the matrices. As these CD-MOFs can dissolve in water to release the metal NPs into solution and also considering the antibacterial Ag and Au NPs and the nontoxic MOFs, these MOF composites are potentially applicable in biomedicines.

Apart from active functional groups, metal nodes in MOFs can also act as redox sites. The oxidation of Ni (II) to Ni (III) sites in Ni-MOF has been employed to reduce the metal ions in MOFs.[70-73] Three Ni(II)-MOFs: $[\{Ni(C_{10}H_{26}N_6)\}_3(bpdc)_3]\cdot 2C_5H_5N\cdot 6H_2O$, $\{[Ni(cyclam)]_2[BPTC]\}_n\cdot 2nH_2O$, and $\{[Ni(cyclam)]_2[TCM]\}\cdot 2DMF\cdot 10H_2O$ have been applied to reduce the metal ions loaded (Ag^+, $AuCl^{4-}$ and Pd^{2+}) in their cavities into the corresponding metal NPs. Ag NPs of ~ 4 nm, Au NPs of ~2 nm and Pd NPs of ~3 nm were synthesized in these three MOFs, respectively.

External stimuli have been widely used to reduce metal ions inside MOFs and yield metal NP/MOF composites. For example, a hydrogenolysis process has been developed to reduce the organometallic precursors inside MOF crystals and generate metal NP/MOF composites. The synthesis of Au NP/MOF-5 with $(CH_3)Au(PMe_3)$ as the precursor,[74] Cu NP/MOF-5 with $(\eta^5\text{-}C_5H_5)Cu(PMe_3)$ as the precursor,[74] Pd NP/MOF-5 with $(\eta^5\text{-}C_5H_5)Pd(\eta^3\text{-}C_3H_5)$ as the precursor,[74] Ru NP/MOF-5 with Ru(cod)(cot) as the precursor,[75] Au NP/ZIF with Au(CO)Cl as the precursor, [76] Ni NP/MesMOF-1 with $NiCp_2$ as the precursor,[77] and Pd NP/MIL-101 with $(\eta^5\text{-}C_5H_5)Pd(\eta^3\text{-}C_3H_5)$ as the precursor [78] have been reported through employing this process. Apart from hydrogenolysis, the metal ion/MOF intermediates also can be reduced by agents such as PVP, $NaBH_4$ and N_2H_4•H_2O to yield the final products, which was exemplified by the formation of Pd NP/MOF-5, [79, 80] Au@Ag core-shell NP/ZIF-8, [81] and Au NP/MIL-101. [82] Additionally, microwave processing is one immerging technique to activate/accelerate chemical reactions and has also been used for the synthesis of MOF composites. Through the irradiation of the specific composites of metal ion/MIL-101 with microwave, Pd-Cu NP/MIL-101 [83] and Cu NP/MIL101[84] composites have achieved. Last but least, heat treatment was also applied to the synthesis of MOF composites. Pd NP/MIL-101 composite has been synthesized by the reduction of Pd^{II}/MIL-101 with the assistant of H_2 at high temperature.[85-87]

2.2.2 Encapsulation of the structures pre-synthesized into MOFs

Many properties of nano-objects are their size, shape and composition related.[88, 89] The impregnation strategy lacks of tuneability on these parameters for the incorporated structures, thus narrows the applications of MOF composites. Novel strategies of encapsulating the nano-objects pre-synthesized with post-formation of MOF shells on their surfaces have been

developed to circumvent this difficulty. The MOF shells can be formed either by post-growth in the MOF growth solution or via chemical conversion of the pre-deposited metal compound structures into MOFs.

2.2.2.1 MOF shell formed by the post-growth

The formation of MOF shells is an interface related process, of which there are three general types: ①the "build-bottle-around-ship" method to encapsulate clusters into MOF composites, ② the selective nucleation and growth of MOFs on the surface of inorganic nanostructure, and ③ the heteroepitaxial growth of MOF shell on another MOF crystal surface.

A typical "build-bottle-around-ship" synthesis procedure has usually been adopted in which the desired catalytic metallo-complex was encapsulated inside the nanopores/channels of porous materials in the presence of synthetic precursors of the porous materials. This method was originally employed to encapsulate metallocomplexes into the cage of zeolites, [90]and has been employed to synthesize MOF composites recently. POMs were chosen as the encapsulated clusters to form the cluster/MOF composites. Su and co-workers have synthesized POM/HKUST-1 composites (NENU-*n*, *n*=1 to 6) by one-step hydrothermal reaction of copper nitrate, 1, 3, 5-BTC, and different kinds of POMs (Figure 4a). [91] NENU-*n* show high thermal stability and the high loading amount of POMs (~50 wt. %) exceeds most traditional POM-supported catalysts. However, copper carboxylate based MOFs usually dissolve in water and this might rule out their practical use for many aqueous phase applications. The more stable POM/MOF composites, POM/MIL-101(Cr) [92] and POM/MIL-100(Fe) [93] were synthesized and these two composites are stable in aqueous solution with no POM leaching. Compared with NENU-*n*, these two composites also show much higher surface areas. The surface area decreases from >1000 m^2 g^{-1} of pure HKUST-1 to ~460 m^2 g^{-1} for NENU-*1*, while the BET values of POM/MIL-101(Cr) and POM/MIL-100(Fe) are almost same with their pure counterparts.

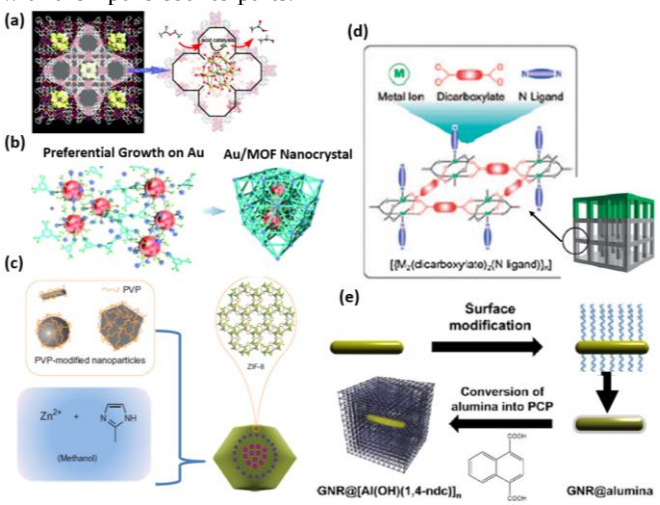

Figure 4. Overview of the methods to encapsulate the pre-synthesized structures into MOFs. (a) The encapsulation of POM clusters into HKUST-1 by "build-bottle-around-ship" method. (b) Au NP/HKUST-1 synthesized by surface modification of MUA. (c) Scheme of the controlled encapsulation of NPs in ZIF-8 crystals with the assistance of PVP. (d) Schematic illustration of the heteroepitaxial growth of MOF@MOF structures with the $[M_2(L)_2(P)]$ (L=dicarboxylate; P=diamine pillar) isoreticular family, and (e)Scheme of the Au NR@MOF composite synthesized by scarified template method. Reproduced with permission.[91, 94, 99, 102, 108]

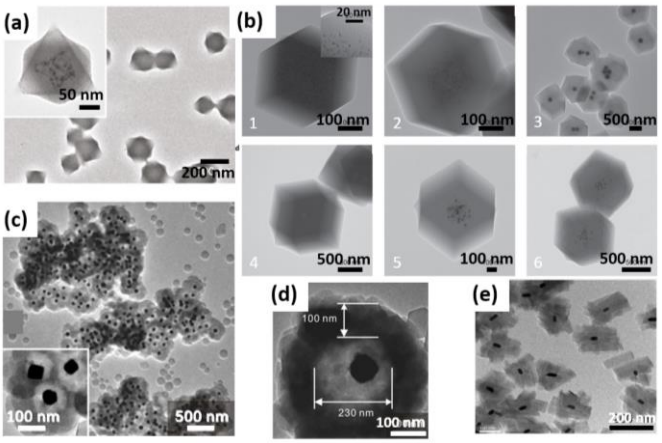

Figure 5. Electron microscopy images of the nanostructures@MOF composites. (a) TEM image of Au NP@HKUST-1. (b) TEM images of ZIF-8 composites containing different types of NPs. (1) and (2) Hybrid crystals containing 3.3 nm Pt NPs. (3) Hybrid crystals containing Ag cubes (~ 160 nm). (4) Hybrid crystals containing 180 nm PVP-modified PS spheres with surfaces that were partially coated with unmodified 13 nm Au NPs. (5) Hybrid crystal containing homogeneously distributed 13 nm Au and 34 nm Au NPs in the central area. (6) Hybrid crystals consisting of 34 nm Au NP-rich cores, 13 nm Au NP-rich transition layers and NP-free shells. (c) Pd nanocrystal@ZIF-8 yolk-shell nanostructures. (d) Enlarged TEM image of the yolk-shell nanostructure. The cores are Pd octahedra with edge sizes of 60 nm, and the shells are microporous ZIF-8 with thickness of~ 100 nm. (d) TEM images of Au NR@$[Al(OH)(1,4\text{-ndc})]_n$ core−shell composite. Reprinted with permission.[94, 99, 101, 108]

To selectively nucleate and grow of MOF shells on the surfaces of incorporated nanostructures, chemical modifications of the functional structures with organic molecules such as surfactants or polymers are often involved. The modified substances are added into the growth solution containing suitable MOF precursors and subsequently MOF shells are constructed around their surfaces. Noble metal NPs are the well-studied species encapsulated due to their broad applications on heterogeneous catalysis and also because of the well-established surface modification techniques of noble metals. Through functionalising the Au NPs with MUA and subsequently transferring them into the Cu^{2+} and 1, 3, 5-BTC mixing solution, Au NP@HKUST-1 core-shell crystals were synthesized (Figure 4b and 5a).[94] Here the symbol @ is adopted from the notation of core-shell nanostructures in nanoscience and nanotechnology.[95] Au NP@MIL-100(Fe) and Pt NP@ZIF-8 composites have also formed by this method.[96, 97] What's more, functional species beyond metal NPs can also be incorporated into MOF crystals through this approach with the suitable surface treatments to trigger the heterogeneous nucleation of MOF crystals. Through heterogeneous nucleation of porous MOF networks on the outer surface of magnetic NPs,

iron oxide NPs have been successfully incorporated into three MOFs (DUT-4, DUT-5 and HKUST-1).[98] Huo's group reported the incorporation of diversified kinds of inorganic nanostructures such as Au NPs, Pt NPs, CdTe NPs, Fe_3O_4 NPs, $NaYF_4$ NPs, Ag Nanocubes, β-FeOOH NRs and even organic nanostructures such as PS nanospheres into ZIF-8 crystals through capping the nanostructures incorporated with PVP before the growth of ZIF-8 shells (Figure 4c and 5b).[99] Meantime, controlled incorporation of multiple species within one ZIF-8 crystallite by this strategy was also demonstrated. In their following paper, this method was further extended to the encapsulation of NPs into other MOFs such as ZIF-7, MIL-53 and MIL-101-NH_2.[100] Using thin Cu_2O layer to activate the heterogeneous nucleation and growth of ZIF-8, Tsung's group has synthesized yolk-shell Pd NP@ZIF-8 structures (Figure 5c).[101] The selective growth of ZIF-8 shell is believed attributable to the similar binding properties expressed by zinc and copper ions to 2-metythylimidazole, which enhance the heterogeneous nucleation and growth of ZIF-8 on the surface of metal NPs.

The growth of MOF shells on the surface of another MOF crystal has also been investigated. Unlike the MOF composites discussed above, the formation of MOF core and MOF shell structures strongly relies on the close lattice mismatch between the two MOFs. Therefore, a heteroepitaxial property is usually shown between the two MOFs and a preferred crystal orientation along the MOF interface to maximize coincidence between the two lattices was observed in the MOF heterostructures. For example, Kitagawa and co-workers have explored the heterometallic epitaxial growth of tetragonal [Cu_2 (ndc) $_2$(dabco)] shell on the pre-formed [Zn_2 (ndc) $_2$(dabco)] MOF surface through a solvothermal reaction of core-MOF in the growth solution of shell-MOF (Figure 4d).[102] A perfect mismatch between [Cu_2 (ndc) $_2$(dabco)] and [Zn_2 (ndc) $_2$(dabco)] at the (100) surface was shown on the synchrotron X-ray diffraction pattern whereas rotational growth of two Miller domains of the shell lattice at the (001) surface with an average rotational angle of 11.7° between them (Figure 6a).

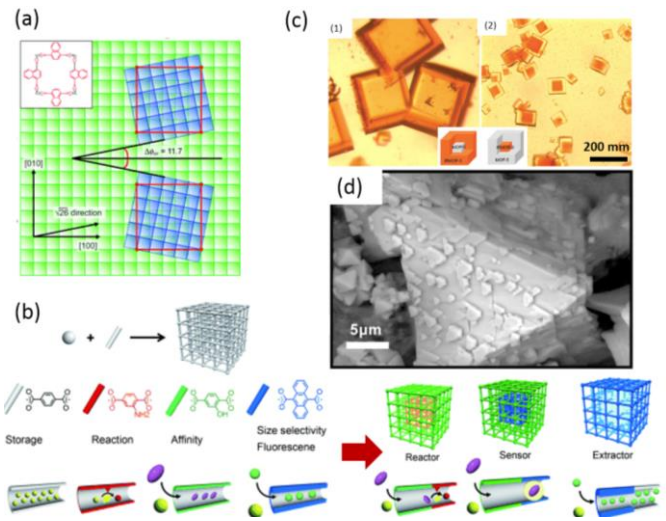

Figure 6. Characterizations of the MOF@MOF structures. (a) Schematic model of the structural relationship between the core lattice [Zn_2(ndc)$_2$(dabco)] and the shell lattice [Cu_2(ndc)$_2$(dabco)] on the (001) surface. The red lines indicate the commensurate lattice between the core lattice and the shell lattice; the (5×5) structure of the core crystal or the (√26 ×√26) structure of the shell. Two Miller domains of the shell crystal are grown on the (001) surface of the core crystal while maintaining the rotational angle ($\Delta\varphi_{av}$ =11.6518), which corresponds to the √26 direction of the (001) surface.(b) MOF crystal hybridization for sequential functionalisation systems. (c) Microscope images of core–shell MOFs (1) IRMOF-3(shell) @MOF-5(core), (2) MOF-5(shell) @IRMOF-3(core). (d) SEM images of the MOF crystals (mixture of bio-MOF-11 and bio-MOF-14. Reprinted with permission. [102, 104, 105, 106]

Apart from metal nodes, the bridging ligands also can be varied to form the MOF core-MOF shell structures which was first demonstrated by Kitagawa's group (Figure 6b).[103,104] Through controlling the location of individual functional ligands, the MOF@MOF structures with spatially separated porous networks of differential pore sizes and chemistries have been synthesized. The combination of small and large pore sizes in one heterogeneous structural crystal provides a simultaneous size selectivity and storage of small molecules. Koh *et al*. have prepared the IRMOF-1/IRMOF-3 core-shell MOF structures which present good colour contrast arising from colourless IRMOF-1 and orange IRMOF-3 and the core-shell structures can be synthesized in both ways (Figure 6c).[105] Li *et al.* have designed and synthesized a mixed MOF composite comprising porous bio-MOF-11/14 and less porous bio-MOF-14 by applying the ligands variation method (Figure 6d).[106]

*2.2.2.2 Chemical conversion of the pre-deposited inorganic structures into MOF*s.

Conversion chemistry is a versatile approach for the conversion of one compositional nanostructure into another. Through the chemical conversion process, metal compound materials which serving both as the source of metal ions and to introduce the interface for MOF growth, have been used for the synthesis of MOFs. Kitagawa and co-workers have employed this method to synthesize Al_2O_3/[Al(OH)(1,4-ndc)]$_n$ composites and Au NR@[Al(OH)(1,4-ndc)]$_n$ NPs by the pseudomorphic replication of Al_2O_3 structures preformed (Figure 4d and 5d).[107, 108] The conversion was realized through the reaction of alumina with the ligand (H_2(1,4-ndc)) under high temperature in microwave reactor. Apart from Al_2O_3, ZnO and Cu_2O were also the conversion materials. ZnO@ZIF-8 NW arrays were formed by partially chemical conversion of the ZnO NW to ZIF-8 in DMF/H_2O or 1-octanol with the assistance of 2-methylimidazole at elevated temperature.[109, 110] As Cu_2O can dissolve gradually in the mildly acidic growth solution of 1,3,5-BTC and direct the growth of HKUST-1, the encapsulation of NPs pre-synthesized into HKUST-1 can be achieved by using NP@Cu_2O core-shell nanostructures as the self-template.[111] With the protection of Cu_2O shell, various NPs (Au NPs, Au NRs, Pd nanocubes, and Pt-on-Au dendritic NPs) could be encapsulated into HKUST-1 easily to form a yolk-shell

structure without being aggregated or dissolved in the reaction mixture. As many metal compounds dissolve in acid or basic conditions to give the metal ions at elevated temperature, also given the facts that diversified kinds of metal compounding core-shell nanostructures have been synthesized, [112] it is expected that this method is widely applicable to the synthesis of different kinds of nanostructure@MOF composites.

2.2.3 Other methods

One-pot synthesis, a strategy to improve the efficiency of a chemical reaction whereby a reactant is subjected to successive chemical reactions in just one reactor, was also applied to the synthesis of MOF composites. Tang's group recently reported the synthesis of Au NP/MOF-5, Au NP/ZIF-8, Au NP/IRMOF-3 and Ag NP/MOF-5 composites through directly mixing and reaction of either the Au or Ag and MOF precursors in the reaction solution containing DMF, PVP and ethanol.[113] Bandosz's group has demonstrated the synthesis of graphite oxide/MOF-5, graphite oxide/HKUST-1 and graphite oxide/Fe-MIL-100 composites through one-pot reactions of the mixing solutions of graphite oxide and the MOF precursors.[114-116] The graphite oxide/MOF-5 composite prefers to adopt a lamellar structure constructed from the alternative layers of graphite oxide and MOF-5. The formation mechanism was explained based on the interactions between the epoxy groups on graphene sheet and the oxide clusters in MOF-5.[117] Similar laminar structures were also observed on the *in-situ* synthesized graphene-porphyrin MOF composite.[118] However, the other graphite oxide/MOF composites synthesized by Bandosz's group, such as the graphite oxide/HKUST-1 and graphite oxide/MIL-100, did not show such hierarchical structures. This architecture deference is believed to attribute to the different growth mechanisms of HKUST-1, MIL-100 and MOF-5 on the surface of graphite oxide.

Apart from one-pot synthesis, solid grinding strategy has also been employed to form MOF composites. Through solid grinding of $(Me)_2Au(acac)$ with the MOF powders and following with H_2 reduction at elevated temperatures, different Au NP/MOF composites (CPL-1, CPL-2, MIL-53, MOF-5, HKUST-1 and ZIF-8) have been synthesized.[119-121]

3. Applications of MOF composites

3.1 Small molecule absorption, storage and separation

3.1.1 Gas absorption and storage

Stimulated by the sharply rising level of atmospheric CO_2, one of the greatest environmental concerns facing our civilization today, [122] the adsorption/capture of CO_2 is becoming one important application of MOF composites. GO/MOF or graphite oxide/MOF composites are well studied on this owing to the synergistic effects for the reactive adsorption of CO_2 correlating to the active sites formed at the interface between graphene layers and the MOFs.[123] The capabilities on the CO_2 absorption are greatly enhanced for ZIF-8 and HKUST-1 when compositing with GO or graphite oxide. The CO_2 uptake increases from 27.2 wt. % (pure ZIF-8) or 33 wt. % (pure GO) to 72 wt. % (ZIF-8 composite with 20 wt. % GO) at 195 K for the GO/ZIF-8 composites.[124] The graphite oxide/HKUST-1 composite shows a CO_2 uptake as high as 4.23 mmol/g at room temperature, which is twice of the pristine HKUST-1 powder and 10 times higher than that of the graphite oxide sample.[125] Apart from CO_2, the absorption and removal of other toxic gases such as NH_3, H_2S and NO_2 by MOF composites have also been investigated.[45,126-128]

Hydrogen storage is another important application of MOF composites. Energy sources with low or no carbon are expected to decrease CO_2 level in environment and hydrogen is one of the most promising candidates. It has an energy density much greater than gasoline and emits no CO_2 after burning. The H_2 uptakes are generally represented as excess and total adsorption amount.[129] Up till now, the highest excess H_2 storage capacity reported so far for MOFs is 99.5 mg g^{-1} at 56 bar and 77 K in NU-100 and the highest total H_2 storage capacity reported is 176 mg g^{-1} (excess 86 mg g^{-1}) in MOF-210 at 77 K and 80 bar.[130-131] Whereas MOFs show high hydrogen uptake at low temperatures, they do not show advantage on hydrogen storage at room temperature compared with other porous materials such as active carbons and zeolites.[132-133] The weak interactions between H_2 molecules and the MOF structures at room temperature are believed one important reason. Therefore, new methods to enhance the interactions of MOFs with H_2 through incorporating functional species have been developed and better hydrogen adsorption performances at room temperature were achieved by these MOF composites.

3.1.1.1 Optimize the pore size distributions of MOFs with the corporation of other porous materials

The large void spaces in MOFs are often not completely utilized for hydrogen storage and these spaces can be optimized through the incorporation of other microporous materials. Carbon materials have been widely used in composite systems for diversified applications. Particularly, CNTs have been used for the preparation of composite materials with enhanced gas storage capacity. The CNT/MOF-5 composite shows not only about 50% increase in the hydrogen storage capacity (from 1.2 to 1.52 wt. % at 77 K and 1 bar and from 0.3 to 0.61 wt. % at 298 K and 95 bar) but also much improved environmental stability in the presence of ambient moisture compared with the pristine MOF-5.[134] The incorporation of SWCNT into MIL-101 also results in an increase of hydrogen storage from 0.23 (pristine MIL-101) to 0.64 wt. % (8 wt. % SWCNT in MIL-101) at 298 K and 60 bar condition.[135] Other carbon materials have also used to enhance the hydrogen uptake of MOF composites. The GO/HKUST-1 composite with GO content of 9 wt. % exhibits about 30% enhancement in H_2 capacity compared with the pristine HKUST-1(from 2.81 wt. % to 3.58 wt. % at 77 K and 42 bar).[136]

3.1.1.2 Enhance the hydrogen storage by "spillover" effect

The *spillover effect* involves the dissociative chemisorption of hydrogen on the surface of metal NPs to atomic hydrogen and its subsequent migration onto adjacent surfaces via diffusion.

Combining this property with the high surface-volume ratio of MOFs, the metal NP/MOF composites are promising materials to enhance hydrogen capacities. Two major approaches to facilitate the hydrogen spillover in MOF composites have been reported: ① building carbon bridges between the dissociative metals and MOFs, and ② direct doping of dissociative metals (Pt, Pd, and Ni) into MOFs.

A carbon bridge between the metal catalyst and MOF can form via the linkage of amorphous carbon through the carbonization of saccharides such as glucose or sucrose. With the bridging of metal catalysts and MOFs, the *spillover effect* takes place on the catalyst surface and the recombination of atomic hydrogen formed is retarded by the MOF channels. Pt NPs are often used to combine with the matrices such as IRMOF-8[137-140] or MIL-101[141] through the bridging reaction. The Pt NP/MOF composites formed show much enhanced hydrogen capacity at room temperature and a capacity of as high as 4 wt.% was achieved at 100 bar for the Pt NP/IRMOF-8, which is much higher than the pristine IRMOFs (usually <1 wt.% at room temperature).

The spillover of hydrogen also takes place in the MOFs with directly doped metals NPs.[53, 68, 142-143] metal NP/MOF composites such as Pd NP/MOF-5, Pt NP/MOF-177, Ni NP/MIL-101, Pd NP/MIL-100(Al) and Pd NP/{[Zn_3 (ntb) $_2$(EtOH) $_2$] ·4 EtOH} $_n$ have been synthesized by the reduction of metal ions inside MOF matrices and these composites show higher hydrogen capacities compared with their counterparts.

Table 1. Gas separation performance of MOF/polymer membranes

MOF/polymer	MOF loading	Permeability	Selectivity	Test conditions
MIL-53(Al)-NH_2 /copolyimide[153]	10-15 wt.%	CO_2, 57-137	H_2/CH_4, 34.7 CO_2/CH_4, 35.8	35 °C, 3 bar
MIL-101(Al)-NH_2/copolyimide[153]	5-10 wt.%	CO_2, 53-151	H_2/CH_4, 67.3 CO_2/CH_4, 42.2	35 °C, 3 bar
ZIF-7/Pebax[154]	8-34 wt.%	CO_2, 41-145	CO_2/CH_4, 44 CO_2/N_2, 105	25 °C, 3.75 bar
Cu-bipy/PSF[155]	0-5 wt.%		H_2/CH_4, ~200 CH_4/N_2, ~10	35 °C, 1 bar
MIL-53(Al)-NH_2/PSF[156]	8-40 wt.%	CO_2, 5	CO_2/CH_4, ~25	35 °C, 3 bar
MIL-101/PSF[157]	0-24 wt.%	O_2, 6	O_2/N_2, 5-6	30 °C, 3 bar
HKUST-1/PSF[45]			H_2/CO_2, 7.2 H_2/C_3H_6, 5.7	25 °C, 2.75 bar
HKUST-1/PPO[158]	10-50 wt.%		CO_2/N_2, ~25 CO_2/CH_4, ~30 H_2/N_2, ~25 H_2/CH_4, ~30	30 °C
ZIF-8/6FDA-durene[159]	33. 3 wt.%	H_2, 2136 N_2,137 O_2,449 CH_4, 140	H_2/CO_2, 12 H_2/N_2,141 H_2/CH_4, 203	35 °C, 3.5 bar
MIL-53 (Al)/polyimide[160]	20-40 wt.%		CO_2/CH_4, 77	
Cu-BPY-HFS /matrimid[34]	10-40 wt.%		CH_4N_2, 1.21	
ZIF-8/matrimid[30]	0-80 wt.%	O_2, 1.13-5.88 CO_2, 4.72-24.55 H_2, 18.07-71.22	H_2/CO_2, 3-4 CO_2/CH_4,44-125	35 °C, 2.7 bar
ZIF-90/6FDA-DAM[31]	15 wt.%	CO_2, 590-720	CO_2/CH_4, 37	25 °C, 2 bar
HKUST-1/matrimid[33]			CO_2/N_2, 23-27	35 °C, 10 bar
HKUST-1/polyimide[161]			H_2/CO_2, CO_2/N_2,	

3.1.1.3 Formation of hydrides

Metal hydrides are also the storage medium of hydrogen. Latroche and Ferey *et al.* reported that the Pd NP/MIL-100(Al) composite shows an increased hydrogen uptake as twice that of the pristine MOF powder at room temperature and 40 bar (the excess hydrogen capacity increases from 0.19 wt.% to 0.35 wt.%).[144] The diffraction peaks of Pd shift with the increase of H_2 pressure, indicating the formation of Pd hydride due to the insertion of hydrogen atoms at the interstitial sites of Pd. It should be noted that the hydride and dehydride processes are not reversible under mild conditions for many metals. Therefore, selecting the suitable metals is one key factor to enhance the hydrogen capability of metal NP/MOF composites. For example, Pt NP/MOF-177 adsorbed 2.5 wt. % of H_2 at room temperature and 144 bar in the first adsorption cycle. The capacity decreased to 0.5 wt. % (close to the pure MOF-177) in the second cycle due to the irreversible dehydride process of Pt hydrides at room temperature.[143]

3.1.2 Liquid adsorption

MOFs have been investigated for the adsorption of harmful materials from liquids and the adsorption efficiency can be greatly enhanced with the introducing of metal ions/clusters or NPs inside MOFs. Jhung's group has systematically studied the remove of sulfur-containing compounds (such as Th, BT and DMDBT) and nitrogen-containing compounds (such as QUI and IND) in fuels by MOF composites. They found that the adsorption capacity of BT by $CuCl_2$-loaded MIL-47 (310 mgg^{-1} for $CuCl_2$ (0.05)/MIL-47) is much higher than that of pure MIL-47 (231 mgg^{-1}) and even higher than that of Cu^I-Y, which once showed the highest capacity before (254 mgg^{-1}).[145] With the loading of CuCl, the adsorption capacities of CuCl/MIL-100(Cr) for QUI and IND have improved by 9% and 15% compared to pristine MIL-100(Cr), respectively.[147] In these two cases, the enhancement of adsorption was explained to attribute to the π-complexation effect of the Cu^+ sites. They also introduced POM clusters into MOFs and the adsorption capacity of basic QUI increased by 20% with 1 wt. % PWA impregnation in MIL-101.[148] Apart from MIL-101, the impregnation of PWA in HKUST-1 also results in an increase by 26% of BT adsorption compared with the pure HKUST-1.[149] Moreover, graphite oxide/MOF composite has also been used for the adsorption studies.[150] The graphite oxide/MIL-101 composite synthesized by Jhung's group shows the highest adsorption capacity for QUI and IND (863 mgg^{-1}) among reported adsorbents so far.

Apart from removing sulphur- and nitrogen-containing compounds in fuels, MOF composites have also been used to adsorb other adsorbates such as ethylene and toluene. The cuprous NP loaded MIL-101 shows an enhanced ethylene adsorption capacity and higher ethylene-ethane selectivity (14.0), compared to pure MIL-101 (1.6).[151] The $PdCl_2$/MIL-101 shows excellent toluene adsorption and an uptake of 660 mgg^{-1} was achieved for the 3 wt. % $PdCl_2$/MIL-101,[152] representing an enhancement of 450% over that of unmodified MIL-101.

3.1. 3 Molecule separation

MOFs are ideal materials for small molecule separation owing to their high surface areas, adjustable pore dimensions, and tuneable surface functionalities. However, given the fragility of MOFs, formation of high quality MOF crystal membranes is still a great challenge. Fabrication of mixed-matrix membranes (MMMs) through the incorporation of MOF crystals with polymeric matrices is an alternative approach to solve this problem. One key advantage of such MMMs is that they have combined the high processibility and mechanical stability of polymers with the excellent gas separation properties of MOF solids. A short summary of current publications on the gas separation performance of MOF/polymer membranes is listed at Table 1.

Apart from gas separation, MOF contained MMMs have also been used for liquid separation. The MMMs with MOFs (HKUST-1, MIL-47, MIL-53(Al) and ZIF-8) as dispersed phases in PDMS have been used for the separation of Rose Bengal (RB) from isopropanol.[37] An increased permeance from 0.54 $L{\cdot}m^{-2}{\cdot}h^{-1}$ bar^{-1}(unfilled PDMS membranes) to 0.7-0.9 $L{\cdot}m^{-2}{\cdot}h^{-1}$ bar^{-1} was reported. Sorribas *et al.* have synthesized MMMs containing a range of 50-150 nm MOF NPs (ZIF-8, MIL-53(Al), NH_2-MIL-53(Al) and MIL-101(Cr)) in a PA thin film layer and the organic solvent nanofiltration of membranes was evaluated on the basis of MeOH, THF permeances and rejection of styrene oligomers.[162]. MeOH and THF permeance increase when the MOF particles were embedded into the PA layer, whereas the rejection remains higher than 90% in all membranes. The permeance is also enhanced with the increase of pore size and porosity of the MOFs. Within all the membranes, the membrane of MIL-101(Cr) (pore size~3.4 nm) leads to an exceptional increase in permeance from 1.5 to 3.9 and from 1.7 to 11.1 $L{\cdot}m^{-2}{\cdot}h^{-1}{\cdot}bar^{-1}$ for MeOH/PS and THF/PS, respectively.

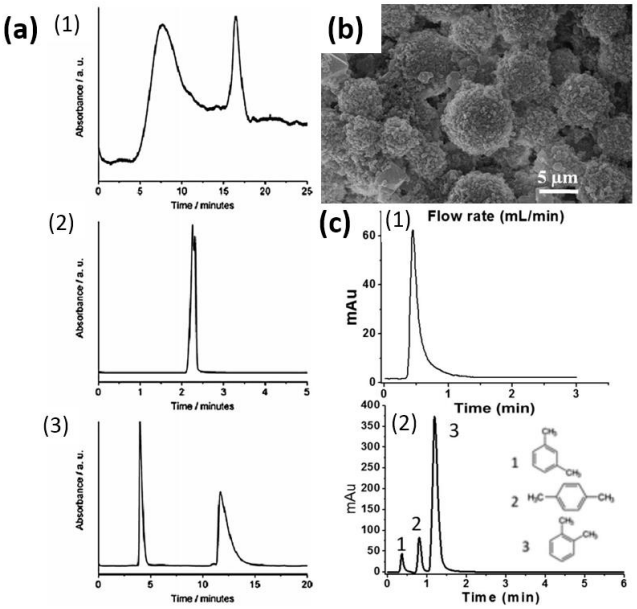

Figure 7. The applications of MOF composites for fast separation. (a) HPLC experiments for the separation of mixtures of ethylbenze and styrene on (1) a pure HKUST-1 column (2) an unmodified column of Nucleosil-100 silica and (3) the HKUST-1-silica composite column. In chromatogram 3, ethylbenzene is eluted first with a retention time of 4.1 min followed by styrene at 12.3 min. The separation factor for this mixture is 5.2. (b) A SEM image of the silica@HKUST-1 particles. (c) (1) The chromatogram showing that the column packed with silica particles cannot separate styrene and ethylbenzene. (C) The chromatogram with silica@HKUST-1 particles packed for the separation of toluene (1), ethylbenzene, (2), and styrene (3). Reprinted with permission.[41, 42]

Through coating on the surface of porous oxide microspheres, MOFs also can be employed as the stationary phases in liquid chromatography in molecule separations. Ameloot *et al*. have prepared silica@HKUST-1 particles for the separation of ethylbenzene/styrene and the particle column shows extremely effective on the separation of ethylbenzene and styrene with relatively low backpressure (Figure 7a).[41]. As the comparison, a pure HKUST-1 column also can separate these components but the peaks are much broad (Figure 7a-1),

while the bare silica column has no observable resolution to them (Figure 7a-2). The separation of toluene/ethylbenzene/styrene and toluene/*o*-xylene/thiophene by silica@HKUST-1 microspheres packed columns has also been demonstrated. (Figure 7b-c).[42] When a pure silica packed column was employed, the three xylene isomers were eluted as a single broad peak (Figure 7c-1). The separation can be easily realized with a silica@HKUST-1 packed column (Figure 7c-2). The silica@ZIF-8 microspheres have also been prepared as the stationary phase and a high column efficiency (23 000 plates m^{-1} for bisphenol A) for the HPLC separation of endocrine-disrupting chemicals and pesticides was achieved.[163]

3.2 Catalysis

MOFs and their composites have emerged as the novel materials with promise in catalysis. The catalytic properties can stem from the MOFs themselves for pure MOF, [14] the incorporated functional species in the MOF composites, or the combination of both. The application of metal NP/MOF composites on heterogeneous catalysis has been fully reviewed by Dhakshinamoorthy and Garcia.[164] Therefore, this paper emphasises on the catalytic properties of MOF composites integrated with other functional species such as clusters and semiconductor NPs which have not been fully reviewed yet.

3.2.1 Catalysis by cluster/MOF composites

POMs are polyatomic ions (usually anions) that consisting of three or more transition metal oxyanions linked together by shared oxygen atoms to form large, closed 3-dimensional frameworks. The huge range of size, structure and elemental composition lead the POMs a wide range of properties. Especially, the high thermal stability and reversibly reducibility of the Keggin ions by accepting electrons make them good catalysts for a range of organic reactions such as epoxidation, alcohol oxidation, sulfoxidation and alkeyl arene oxidation.[165] However, the low specific surface area, low stability under catalytic conditions and high solubility in aqueous solution restrict their catalytic applications. Owing to the higher surface area, enhanced chemical stability and ease to reuse of the POM/MOF composites compared with pristine POMs, the formation of POM contained MOF composites have attracted much attention.

Hydrolysis of ester in excess water was employed as a demonstration of the catalytic properties of POM/HKUST-1 composites ((NENU-*n*, *n*=1-6)).[91] The NENU-*n* show a superior catalytic activity compared to most inorganic solid acids. Among all the synthesized NENU-*n* composites, NENU-*3a* has a highest catalytic activity of 313.8 mmol $mol_{acid.}^{-1}$ min^{-1} which even exceeds the best prior results of 275 mmol $mol_{acid.}^{-1}$ min^{-1} obtained by $H_3PW_{12}O_{40}$ immobilized in organomodified mesoporous silica.[166] The conversion of ethyl acetate reaches a maximum of >95% at ~ 7 h (Figure 8a).[91] The $PMo_{12-n}V_n$ (*n*=1-3)/HKUST-1 composites were applied to the liquid hydroxylation of benzene with O_2 and the phenol yield can reach up to 7.37% in 20 min and a high TOF of 44.2 h^{-1} was obtained.[167] A comparison of the catalytic capabilities between POM/MOF and zeolite has been carried out through the esterification reaction of acetic acid with 1-propanol (Figure 8b). POM/HKUST-1 outperforms zeolite Y and shows an as high as 30% conversion rate after 7 hours, comparing with only 15% conversion in 7 hours for zeolite Y.[168] Moreover, the POM/HKUST-1 composites also exhibit higher catalytic performances than the pure HKUST-1, or γ-Al_2O_3, and γ-Al_2O_3 supported POM catalysts (Figure 8c). The dehydration of methanol to dimethyl ether was employed to investigate the effect of particle size of POM/HKUST-1 on their catalytic activities.[169] NENU-*1* with average particle diameters of 23, 105, and 450 μm were prepared and it is interesting to note that the reaction can be carried out at a lower temperature when NENU-*1* (23 nm) was used as the catalyst. Moreover, even the cheap methanol with high water content can be used as the starting material when NENU-1 (23 nm) particles were used.

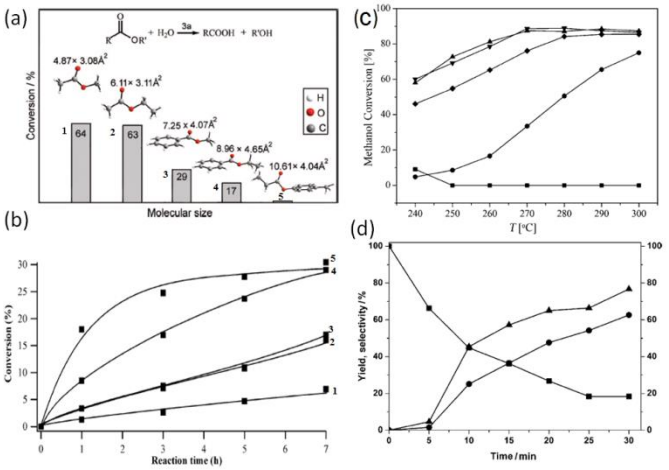

Figure 8. The catalytic capability of POM/MOF composites. (a) Results for the hydrolysis of ester in the presence of NENU: 1) methyl acetate; 2) ethyl acetate; 3) methyl benzoate; 4) ethyl benzoate and 5) 4-methyl-phenyl propionate. (b) Esterification reaction of acetic acid with 1-propanol. Conversion of acetic acid (1) without catalyst, on (2) hydrothermally synthesized micron-sized HPW/$Cu_3(BTC)_2$, (3) ultrastable Y zeolite (4) 65 nm-sized HPW/$Cu_3(BTC)_2$ and (5) 50 nm-sized HPW/$Cu_3(BTC)_2$ catalysts. (c) Conversions of methanol dehydration to DME over catalysts of (■) $Cu_3(BTC)_2$, (●) γ-Al_2O_3, and NENU with the average particle diameters of (▼) 23, (▲) 105, and (♦) 450 μm at the pressure level of 0.6 MPa and LHSV of 2 h^{-1}. (d) Yields and selectivities over time for fructose dehydration using PTA(3.0)/MIL-101 in DMSO at 130°C; ■ fructose retention, ●HMF yield, ▲ HMF selectivity. Reprinted with permission.[91, 168, 169, 171]

As the copper carboxylate based MOFs degrade in water, [170] researchers started to replace HKUST-1 with chemically more stable MOFs such as MIL-101. PTA ($H_3PW_{12}O_{40}$) was encapsulated into MIL-101(Cr) and its catalytic capabilities on the selective dehydration of fructose and glucose to HMF have been tested.[171] An HMF yield of 79 % from fructose was obtained after 2.5 h and the TOF of the solid catalyst (reaction time of 10 min) was about 350 h^{-1}. The HMF yield was 63 % and the selectivity was 77 % after 0.5 h for the dehydration of glucose (Figure 8d). This PTA/MIL-101(Cr) also can be

recycled under the same reaction conditions. Moreover, the POM/MIL-101(Cr) also shows the highest catalytic activity (TOF >656 h^{-1}) in all the literatures so far in the Knoevenagel condensation between benzaldehyde and ethyl cyanoacetate in solvents such as toluene, DMF and ethanol at 313 K.[78]

3.2.2 Catalysis by semiconductor/MOF composites

The applications of MOFs on light harvesting have attracted much attention recently. Apart from designing the MOFs with photoactivities such as UiO-66,[172] amino-functionalised Ti(IV)MOF[173] and Ru-based MOFs,[174] an alternative way is the formation of semiconductor/MOF heterostructures with better capability on light harvesting owing to the synergistic effect. Although porphyrin-based MOFs are attractive for solar photochemistry applications, their absorption bands provide limited coverage in the visible spectral range. Jin *et al.* have functionalised an porphyrin-based MOF with CdSe/ZnS core/shell QDs for the enhancement of light harvesting via energy transfer from QDs to the MOF.[175] This sensitization approach results in a >50% increase in the number of photons harvested by a single monolayer MOF structure with a monolayer of QDs on the surface of MOF. By solvothermal reaction of $Cd(Ac)_2 \cdot 2H_2O$ in DMSO with the presence of MIL-101 crystals, CdSe NP/MIL-101 composite has been synthesized and the embedding of CdS NPs significantly increases the photocatalytic efficiency of the composite in the reaction of visible-light-promoted photocatalytic hydrogen production. The rate of H_2 evolution increases from no detectable H_2 evolution of the pristine MIL-101 to a maximum of ~150 μmol h^{-1} after embedding of CdS NPs on MIL-101.[176]

3.3 Biomedical applications

MOFs can be designed to response to the external stimuli such as heat, light, magnetic force, etc. The resulted microstructure evolutions show implications on the disease therapy and the signal produced can be analysed for the health diagnosis. The review by Horcajada *et al.* has provided a detailed discussion on pure MOFs as drug carriers (including the cytotoxicity of MOFs, the interactions between MOFs and the loaded molecules, and the controllable drug release by the designed MOF structures).[17] Therefore, this section emphasises on the bio-applications of MOF composites, which could be MOFs with surface coating to enhance their bio-compatibility or MOFs with nanostructures embedded to introduce more functionalities.

3.3.1 Biomedical imaging

Silica/polymer coated MOFs have been studied in biomedical imaging owing to the unique fluorescence and magnetic properties of MOFs.[177] Silica coated phosphorescent ruthenium MOF [Ru-{5,5'-$(CO2H)_2$-bpy}$(bpy)_2$]$(PF_6)_2$([L-H_2]$(PF_6)_2$) with high dye loadings has been synthesized by Liu and co-workers and the targeting efficiency of this material was further improved by coating with PEG–AA.[50] This MOF composite is an efficient optical imaging contrast agent and exhibits excellent cancer specificity as demonstrated by the uptake studies and confocal microscopy of H460 cells *in vitro* (Figure 9a). Significant MLCT luminescent signal was observed in the confocal z section images for H460 cells incubated with the MOF composite and less luminescence was observed for H460 cells incubated with the non-targeted MOF. Through further functionalization of the silica shell with contrast agents, MOF composites with multimode imaging properties have been achieved. The Ln $(BDC)_{1.5}(H_2O)_2$ (Ln= Eu^{3+}, Gd^{3+}, or Tb^{3+} and BDC=1, 4-benzenedicarboxylate) MOFs with the surface modification of a silylated Tb-EDTA monoamide derivative (3'-Tb-EDTM), can selectively detect DPA, a major constituent of many pathogenic spore-forming bacteria, in the presence of biologically prevalent interferences such as amino acids.[178] Through the attachment of multifunctional polymer chains to Gd-MOF NPs, a novel theragnostic device with the bi-functions of tumour targeting and diagnostic imaging was prepared by Rowe and co-workers.[179] Apart from imaging, the MOF NPs also show dose-dependent inhibition of growth of the FITZ-HSA tumour cells in the cell growth inhibition studies.

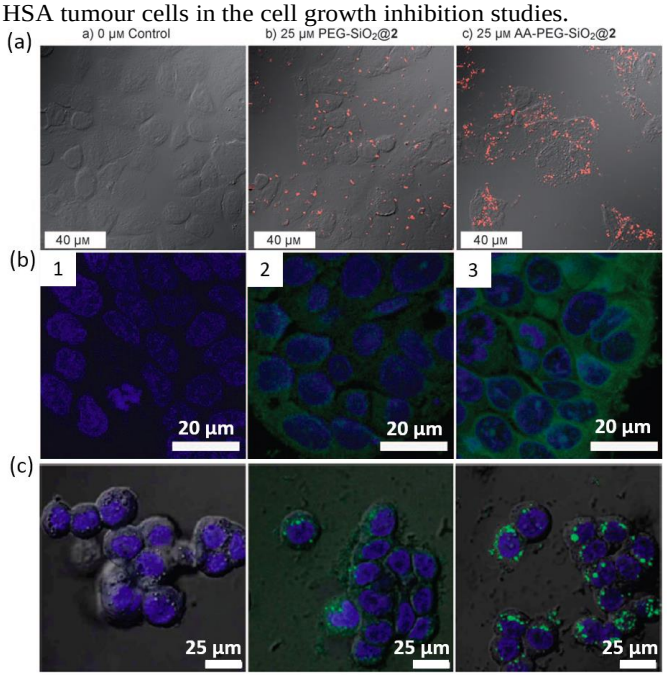

Figure 9. The applications of MOF composites on bio-imaging. (a) Confocal microscopy images of H460 cells that have been incubated without any particles (1), with PEG-SiO_2 coating (2) and with AA-PEG-SiO_2 coating (3). (b) Merged confocal images of HT-29 cells that were incubated with different MOF NPs. The blue colour was from DRAQ5 used to stain the cell nuclei while the green colour was from Rhodamine-B. (c) Overlayed DIC and confocal fluorescence images of the DRAQ5channel (blue, nuclear stain) and the BDC-NH-BODIPY channel (green) of HT-29 cells incubated with no particles (left), 0.19 mg/mL of NPs (equivalent to 17 μM BODIPY) (middle), and 0.38 mg/mL of NPs (equivalent to 34 μM BODIPY) (right).Reprinted with permission.[50, 51,180]

The MOF@sillica core-shell NPs have also been used for the bio-imaging and drug delivery simultaneously. A preliminary work on the utilization of MOF composites in MRI and anticancer drug delivery has been reported by Lin's

group.[51] They synthesized silica coated Mn-BDC MOF NPs and functionalized them with both fluorophore and cell-targeting peptide. These particles display large transverse relativities (R_2) of 112.8 $mM^{-1}s^{-1}$ on a per NP basis. Meanwhile, the MOF particles with the targeting peptide also show enhanced uptake of c (RGDfK) compared with those without the targeting peptide, which was confirmed by the confocal image studies (Figure 9b).[51] In their following paper, the loading of organic fluorophore and anticancer drug via covalent modifications of the as-synthesized MOF NPs and the utilization of such system in optical imaging and anticancer therapy have been demonstrated *in vitro* (Figure 9c).[180] Laser scanning confocal microscopy studies on the HT-29 human colon adenocarcinoma cells show fluorescent labelling in a dose dependent manner. The BODIPY fluorescence is present in cells incubated with MOF NPs but absent in cells without the MOF NPs.

3.3.2 Drug delivery

MOFs have been widely studied as drug carriers in which the delivery process of medicines by intrinsic MOFs and the toxicity of MOFs are the main concerns to be investigated. However, the manipulation of delivery and release pathways of drugs which is critical during the therapy, has not been fully investigated in MOF systems yet. Thus, this section emphasises on this immerging field and discusses the methods have been employed to control the drug delivery and release in MOFs.

Although bio-recognition by MOFs has been reported, [51] the manipulation of intrinsic MOF *drug cargo* by magnetic forces has not been reported owing to the restricted cooperative interactions in inorganic-organic network of MOFs. The combination of MOFs with magnetic NPs becomes an alternative solution to circumvent this difficulty. Upon conjugation with target-specific biomolecules, the magnetic NPs can travel in human bodies via blood or lymphatic vessels and recognize desired biological targets. Meanwhile, magnetic NPs also can direct therapeutic agents to a localized target by focusing an external magnetic field to the region.[181] The magnetic NPs will heated up when subjected to a magnetic AC field due to the losses during magnetization reversal process of the particles.[182] The implication of magnetic hyperthermia to heat up MOFs was first demonstrated by Kaskel *et al.* through triggering the release of drugs loaded in the γ-Fe_2O_3 NP/HKUST-1 composite by magnetic forces (Figure 10a).[98] The magnetic field induces heating of γ-Fe_2O_3 NPs which was monitored at a frequency of 183 kHz and a specific absorption rate (SAR) of 11.1 W g^{-1} was calculated from the slope of the curve which is equivalent to 105.7 W g^{-1}(Fe) (Figure 10b). As the comparison, they also loaded HKUST-1 with ibuprofen using a wet infiltration technique and measured its release rate under different temperatures in the control experiment, which shows the significantly accelerated release rates at higher temperatures.

Apart from magnetic hyperthermia, local heat also can be converted from the NIR light irradiation through the photothermal effect.[183] The manipulation of the molecule release from MOFs by utilising photothermal effect has been demonstrated by the NIR light controlled anthracene release from Au NR@ $[Al(OH)(1,4\text{-ndc})]_n$ composite.[108] The release rate of anthracene from the channel of $[Al(OH)(1,4\text{-ndc})]_n$ was enhanced by the heat produced through the highly efficient conversion of optical energy by Au NRs (Figure 10d). The intensity of anthracene in the solution after 120 min was 13.4 times higher than the one without irradiation. Without the Au NR inside, the fluorescence intensity maxima measured after 120 min for the irradiated sample was only 1.4 times higher than the one without irradiation. Therefore, the burst release of anthracene unambiguously attributes to the local heating generated by the Au NRs through photothermal conversion. Given the abundant kinds of bio-molecules/drugs can be loaded in MOFs and the possibility to spatially control their release during the travel in body via local heating, these two strategies will show broad applications in the field of cell biology and clinic therapy.

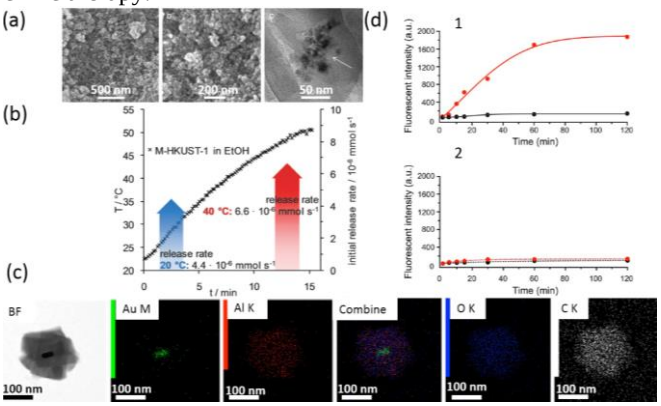

Figure 10. The applications of MOF composites on drug delivery. (a) SEM and TEM images of HKUST-1-magnetite composite. (b) Magnetic heating curve of 324 mg (a) in 30 ml of ethanol at 183 kHz and a field strength of 1.7 kA m^{-1}, giving a specific absorption rate (SAR) of 114.2 W g^{-1} based on the Fe content (X).The arrows indicate the initial release rates for ibuprofen at 20 and 40 ºC, respectively. (c) EDX elemental mapping images of single Au NR@$[Al(OH)(1,4\text{-ndc})]_n$ core−shell composite. (1) TEM image of composite and elemental mapping images by (2) Au, (3) Al, (4) all merged, (5) O, and (6) C. (d) Evaluation of anthracene release from (1) core−shell composites and (2) $[Al(OH)(1,4\text{-ndc})]_n$ crystals without Au NRs. The graphs show linear plots for fluorescence intensity maxima of the released anthracene versus time with (red) and without (black) NIR light irradiation. Reprinted with permission.[98, 108]

3.4 Electrical applications

A combination of the high porosity of MOFs with protonic/electronic conductivity should open up a range of new applications such as electrical-sensors and fuel cells. However, MOFs are typically poor conductors because their metal nodes are not in a redox-active form and most organic ligands used in MOF synthesis do not facilitate electron transfer.[184] Strategies to synthesis the MOFs with enhanced conductivity rely on the use of redox-active metal centres or/and organic linkers,[185] or electron donor and acceptor building blocks,[186] which suffering

from some serious limitations in terms of structural integrity upon redox changes and the conditions to active their conductivities.

To enhance the protonic conductivity of MOFs, Kitagawa's group has developed a hybridization method by filling the MOF channels with proton-carrier molecules such as imidazole or histamine (Figure 11a).[187, 188] The synthetic proton-conducting MOFs usually show the conductivity ranging from 10^{-3} to 10^{-7} S/cm.[189, 190] Owing to the strong host–guest interactions, the proton-carrier molecule/MOF composite can generate a good proton-conductivity larger than 10^{-3} S/cm at high temperatures.

To enhance the electrical conductivity of MOFs, GO, which can be reduced to form rGO, has been used for the synthesis of MOF composites. The combination of high surface area, abundant functional groups of MOFs with the good carrier conductivity and thermal stability of rGO makes their composites well suitable for electrocatalysis.[191] Through functionalising the GO surface and using it as the interlayer for MOF growth, Loh's group has synthesized the graphene-porphyrin MOF composite (Figure 11b).[118] This composite exhibits catalytic activity towards the ORR in alkaline medium with an onset potential of ca.0.93 V vs. RHE. The incorporation of G-dye into the MOF, as opposed to physical mixing of G-dye and MOF, offers better electrocatalytic behaviour (Figure 11b-3) owing to the unique structure of the graphene-porphyrin MOF hybrid where G-dye interconnects with the Fe-MOF in a 3-D manner. Moreover, the large bond polarity and framework porosity of this MOF composite affords a near 4-electron ORR pathway. Compared with the commercial Pt catalyst, this porphyrin-MOF composite possesses a much higher selectivity for ORR and a significantly reduced methanol crossover effects. In the following paper, they also synthesized a GO-copper cantered MOF composite.[192] Due to the unique porous scaffold structure, improved charge transport and synergistic interactions between the GO and MOF, the GO-incorporated Cu-MOF composite exhibits smaller overpotentials and higher current for all three electrocatalytic reactions (HER, OER and ORR) and better stability in acid media compared with the intrinsic Cu-MOF. Moreover, the GO-incorporated Cu-MOF composite delivers a power density that is 76% of the commercial Pt catalyst in polymer electrolyte membrane fuel cell testing which implies that this material is potentially a lower cost substitute to previous reported noble metal catalysts.

Owing to the molecular sieving property of MOFs, their composites also show the implications on molecule sensing and detection. The application of MOF composites on electrical sensing has been demonstrated through the detection of H_2O_2 in buffer solution by the ZnO@ZIF-8 NR arrays (Figure 11c).[109] H_2O_2 is much smaller in size than the aperture of ZIF-8 and its easy penetration induces the enhancement of the photocurrent response (Fig. 11c-2 and 11c-3) while ascorbic acid, a larger molecule, cannot penetrate the MOF shell and leads to the decrease of the current, which confirmed that the ZnO@ZIF-8 NR arrays have distinct PEC response to the hole scavengers with different molecule sizes. Moreover, the positive influence of H_2O_2 on the PEC response of ZnO@ZIF-8 NRs is linear to the concentrations of H_2O_2 within a certain range, indicating that the as-prepared MOF array can be used as the PEC-based sensor.

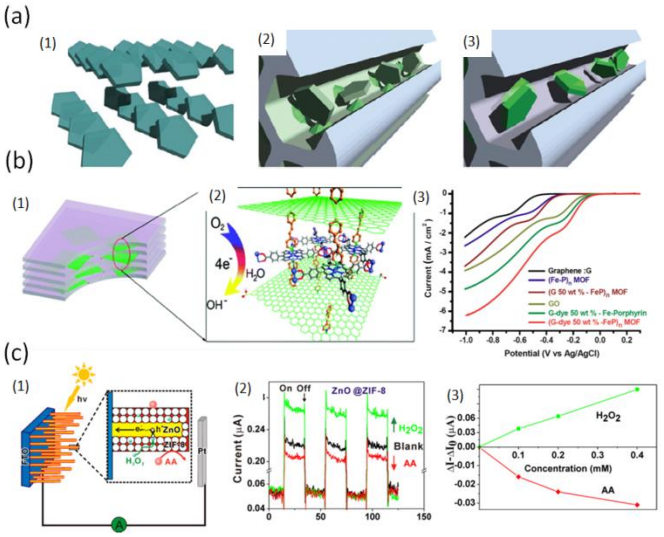

Figure 11. The electrical applications of MOF composites. (a) Imidazole molecules are densely packed with a low mobility that adversely affects the proton-transport process. (1) This occurs in the bulk solid. (2) Imidazole accommodated in a nanochannel containing the active site with a high affinity to imidazole. The strong host–guest interaction retards the mobility of imidazole to afford the low proton conductivity. (3) Imidazoles are accommodated in a nanochannel without strong host–guest interaction, and therefore, the molecules obtain the high mobility to show high proton conductivity. (b) The schematic structures of graphene-porphyrin MOF composite and its DE voltammograms of Graphene, (Fe-P)n MOF, (G 50 wt % -FeP)n MOF, G-dye 50 wt % -Fe-Porphyrin, (G-dye 50 wt % -FeP)n MOF and GO at a rotation rate of 2000 rpm. (c) Schematic diagram of the PEC sensor with selectivity to H_2O_2, Photocurrent responses of the ZnO@ZIF-8 NR array in the presence of H_2O_2 (0.1 mM) and AA (0.1 mM) and $\Delta I - \Delta I_0$ curves in the presence of H_2O_2 and AA with the concentrations as functions. Reprinted with permission.[188, 118, 109]

4. Conclusions

With more than twenty years' development, MOF studies are shifting from the design and synthesis of functional crystal structures to the application and commercialization of MOFs and their derivatives. Composite formation is one alternative way to broaden the application scopes of MOFs from gas absorption, separation and catalysis to new fields such as vapour sensing, drug delivery, electrical applications and even beyond. As the MOF structures may be destroyed during the formation of composites, the stability and activity of MOFs under processing conditions are the key points to be addressed. The MOFs must be retained with high surface area, ordered framework structure and fully accessibility of their pores to the substrates and reagents. Therefore, before and after the formation of MOF composites, the materials should be characterized correctly to confirm their stability. XRD of the pristine MOFs and their composites should be compared to evidence that the crystal structures of MOFs were remained. The data about surface area and pore volume would be given by

nitrogen isothermal adsorption measurement before and after processes.

Although much effort has been dedicated to the study of composite formation strategies, some drawbacks of these approaches restrict their potential utilizations. Given the facts that abundant kinds of ligands with reducing functional groups and polyvalent metal nodes are available for the MOF synthesis, it might be expected that the auto-redox strategy is widely applicable to the synthesis of diversified kinds of metal NP/MOF composites. However, the MOF structures after the compounding process may degrade due to the oxidation of the functional groups or metal nodes as both of which can induce the collapse of the micropores. Moreover, the amount of NPs in the MOF composites is restricted by the maximum loading of metal ions in incipient wetness filtration and ion exchange strategies. The solubility of the precursors in solution and the immersing time of the MOF powders determine the amount of metal ions loaded for incipient wetness filtration and the maximum loading in ion-exchange strategy depends on the amount of active sites in MOFs. Therefore, increasing the metal NP loading and avoiding their aggregation in MOFs simultaneously become one of the main challenges on the synthesis of metal NP/MOF composites.

In order to realize the high performance separations for industry applications, many improvements are required on the preparation of MOF contained MMMs. The size, dispersion of MOF particles and their interactions in the matrices are critical to the synthesis of high quality MOF MMMs. The high homogeneity and dispersion of MOF particles will improve the capability of separation of the membranes. Thus the surface functionalized, size-tuneable MOF particles are highly demanded. However, the study on this is only at its infant stage and more effort should be dedicated in the future.[193] Another key challenge on the fabrication of MOF MMMs is the trade-off between gas selectivity and permeability. The permeability of the MOF MMMs usually decreases with the increase of MOF content when small pore sized MOFs were used, while the gas selectivity enhances owing to the molecular sieve effect of the MOF crystals.[194] The trend is adverse when MOFs with large pores were used.[34] Moreover, the affinity of functional groups and the open metal sites in MOFs should also be considered in the applications of gas storage and separation. For example, due to the interaction of the quadrupole moment of CO_2 with localized dipoles generated by heteroatom incorporation, the polarizing groups such as $–NH_2$ and $-CF_3$ have strong affinity to bind with CO_2.[194] Open metal sites can also enhance the CO_2 adsorption by serving as effective binding sites in the MOF materials.[12] Meanwhile, engineering of the interface between dispersed MOF particles and the matrices is also one challenge on the synthesis of high quality MOF MMMs.[195] As has been discussed in section 2.1, solvent-involved strategies are often employed to the fabrication of MOF MMMs which may induce the formation of uncontrollable voids in the composites. Therefore, solvent-free processes to enhance the adhesion between MOF/polymer interfaces are wanted.

The investigations on the new properties of MOF composites owing to the coupling and synergy affect that originated from the collective interactions between the two constituents are very rare. For example, oxide-supported metal NP/cluster catalysts are essential components of many important chemical processes required by modern industrial economies.[196] Fundamental understanding of the roles of supported oxide in the reactions has been intensively studied. Compared with metal oxides, MOFs show richer surface chemistries and coupling effects can happen in the MOF channels when reactions catalysed by MOF composites are taken place. However, the research on the catalytic properties of metal NP/MOF and cluster/MOF composites is just at its early stage nowadays and a deep understanding of the possible interactions between MOFs and NPs/clusters during the catalytic reactions is still a long-term vision.

Lastly, simulation is becoming an indispensable tool for MOF design and applications by taking advantage of high-speed calculations of today's computer that can accelerate the generation of new insights.[197] Currently simulations are mainly emphasised on the studies of adsorption of gases such methane, hydrogen, and acetylene in pristine MOFs. Given the fast development of MOF composite materials on molecule storage and separation, more effort on the simulation should be made to guide the design and optimize of MOF composite materials for better properties.

In summary, by the combination of MOFs and other functional species, the MOF composites synthesized show enhanced gas absorption, separation, storage capability and catalytic properties. Furthermore, the interaction of functional components/matrix materials with MOF structures can also widen the applications of MOF composites to new fields such as drug delivery/release, fuel cells and electrical catalysis. Although many challenges still remain, it is highly expected that the sustained research effort towards this exciting field will lead the practical applications of MOF composites to be realized in the future.

LIST OF ABBREVIATIONS

AA	ascorbic acid
BET	Brunauer-Emmett-Teller
BGF	benzoic-acid functionalized graphene
Bpdc	4,4'-biphenyldcarboxylate
BPTC	1,1'-biphenyl-2,2',6,6'-tetracarboxylic acid
BPY	4,4'-bipyridine
BT	benzothiophene
CHQ	calix[4]hydroquinone
CNT	carbon nanotube
CPO	coordination polymer of Oslo
CSPs	chromatographic stationary phases
CVD	chemical vapour deposition
Cyclam	1,4,8,11-tetraazacyclotetradecane
DAP	dipicolinic acid
DMDBA	dimethyldibenzothiophene
DMF	N, N-dimethylformamide
DXP	N,N-bis(2,6-dimethylphenyl)-3,4:9,10-perylene tetracarboxylic diimide
FIrpic	2-carboxypyridyl)bis(3,5-difluoro-2-(2-pyridyl)phenyl)iridium(III)

FTO	fluorine doped tin oxide
GO	graphene oxide
HCM	hierarchical porous carbon monolith
HER	hydrogen evolution reaction
HIPEs	high internal phase emulsions
HKUST	Hong Kong University of Science and Technology
HMF	5-Hydroxymethylfurfural
HPLC	High-performance liquid chromatography
IND	indole
LBL	lay-by-layer
MIL	Material of Institute Lavoisier
MLCT	metal-to-ligand charge transfer
MOF	metal-organic framework
MRI	magnetic resonance imaging
MTX	methotrexate
MUA	11-mercaptoundecanoic acid
NIR	near-infrared region
NP	nanoparticle
NT	nanotube
NW	nanowire
OER	oxygen evolution reaction
ORR	oxygen reduction reaction
PA	polyamide
PAM	polyacrylamide
PDMS	polydimethylsiloxane
PEC	Photoelectrochemical
PI	polyimide
PMMA	polymetylmethaacrylate
POM	polyoxometalate
PS	polystyrene
PSU	polysulfone
PTA	phosphotungstic acid
PU	polyurethane
PVA	poly (vinyl acetate)
PVP	polyvinylpyrrolidone
QD	quantum dot
QUI	quinoline
SEM	scanning electron microscope
SWCNT	single-wall carbon nanotube
TCM	tetrakis[4-(carboxyphenyl)oxamethyl]methane
TEM	transmission electron microscope
TEOS	tetraethyl orthosilicate
TGA	thermogravimetric analysis
Th	thiophene
TOF	turnover frequency
UIO	University of Oslo
UMCM	University of Michigan crystalline material
ZIF	Zeolitic Imidazolate Framework

Acknowledgements

S. Z. Li would like to thank the support of the start-up fund of Nanjing University of Posts & Telecommunications (NY213098) and the National Science Foundation of China (GZ213054).

Notes and references

[a] Institute of Advanced Materials (IAM), Nanjing University of Posts & Telecommunications, 9 Wenyuan Road, Nanjing, China
E-mail: iamszli@njupt.edu.cn
[b] Institute of Advanced Materials (IAM), Nanjing Tech University, 30 South Puzhu Road, Nanjing, China
E-mail: iamfwhuo@njtech.edu.cn

1 L. Samain, F. Grandjean, G. J. Long, P. Martinetto, P. Bordet, J. Sanyova, D. Strivay, J. Synchrotron Radiat. 2013, **20**, 460.
2 B. F. Hoskins, R. Robson, *J. Am. Chem. Soc.* 1989, **111**, 5962.
3 B. F. Hoskins, R. Robson, *J. Am. Chem. Soc.* 1990, **112**, 1546.
4 D. Venkataraman, G. B. Gardner, S. Lee, J. S. Moore, *J. Am. Chem. Soc.* 1995, **117**, 11600.
5 G. B. Gardner, D. Venkataraman, J. S. Moore, S. Lee, *Nature* 1995, **374**, 792.
6 O. M. Yaghi, G. M. Li, H. L. Li, *Nature* 1995, **378**, 703.
7 S. Subramanian, M. J. Zaworotko, *Angew. Chem. Int. Edit.* 1995, **34**, 2127.
8 H. Lu, L. Bai, W. Xiong, P. Li, J. Ding, G. Zhang, T. Wu, Y. Zhao, J. Lee, Y. Yang, B. Geng, Q. Zhang. *Inorg. Chem.*, 2014, **53**, 8529.
9 J. Gao, K. Ye, L. Yang, W. Xiong, L. Ye, Y. Wang, Q. Zhang. *Inorg. Chem.*, 2014, **53**, 691.
10 M. P. Suh, H. J. Park, T. K. Prasad, D. W. Lim, *Chem. Rev.* 2012, **112**, 782.
11 H. H. Wu, Q. H. Gong, D. H. Olson, J. Li, *Chem. Rev.* 2012, **112**, 836.
12 K. Sumida, D. L. Rogow, J. A. Mason, T. M. McDonald, E. D. Bloch, Z. R. Herm, T. H. Bae, J. R. Long, *Chem. Rev.* 2012, **112**, 724.
13 J. R. Li, J. Sculley, H. C. Zhou, *Chem. Rev.* 2012, **112**, 869.
14 M. Yoon, R. Srirambalaji, K. Kim, *Chem. Rev.* 2012, **112**, 1196.
15 J. Gao, L. Bai, Q. Zhang, Y. Li, G. Rakesh, J. Lee, Y. Yang,Q.Zhang.*Dalton Trans.*, 2014, **43**, 2559.
16 L. E. Kreno, K. Leong, O. K. Farha, M. Allendorf, R. P. Van Duyne, J. T. Hupp, *Chem. Rev.* 2012, **112**, 1105.
17 P. Horcajada, R. Gref, T. Baati, P. K. Allan, G. Maurin, P. Couvreur, G. Ferey, R. E. Morris, C. Serre, *Chem. Rev.* 2012, **112**, 1232
18 J. Gao, J. Miao, P. Li, W. Teng, L. Yang, Y. Zhao, B. Liu, Q. Zhang. *Chem. Commun*., 2014, **50**, 3786.
19 N. Stock, S. Biswas, *Chem. Rev.* 2012, **112**, 933.
20 Z. Q. Wang, S. M. Cohen, *Chem. Soc. Rev.* 2009, **38**, 1315.
21 S. M. Cohen, *Chem. Rev.* 2012, **112**, 970.
22 Q. Zhu, Q. X. *Chem. Soc. Rev*., 2014, **43**, 5468.
23 I. Ahmed, S. Jhung. *Mater. Today*, 2014, **17**, 136.
24 D. Bradshaw, A. Garai, J. Huo, *Chem. Soc. Rev.* 2012, **41**, 2344.
25 O. Shekhah, J. Liu, R. A. Fischer, C. Woll, *Chem. Soc. Rev.* 2011, **40**, 1081.
26 K. K. Chawla. Composite Materials: Science and Engineering, Third Edition, Springer.
27 F. Millange, C. Serre, N. Guillou, G. Ferey, R. I. Walton, *Angew. Chem. Int. Edit.* 2008, **47**, 4100.
28 G. Li, V. Shrotriya, J. S. Huang, Y. Yao, T. Moriarty, K. Emery, Y. Yang, *Nat. Mater.* 2005, **4**, 864.
29 T. Ben, C. J. Lu, C. Y. Pei, S. X. Xu, S. L. Qiu, *Chem.-Eur. J.* 2012, **18**, 10250.
30 M. J. C. Ordonez, K. J. Balkus, J. P. Ferraris, I. H. Musselman, *J. Membr. Sci.* 2010, **361**, 28.
31 T. H. Bae, J. S. Lee, W. L. Qiu, W. J. Koros, C. W. Jones, S. Nair, *Angew. Chem. Int. Edit.* 2010, **49**, 9863.
32 E. V. Perez, K. J. Balkus, J. P. Ferraris, I. H. Musselman, *J. Membr. Sci.* 2009, **328**, 165.
33 S. Basu, A. Cano-Odena, I. F. J. Vankelecom, *J. Membr. Sci.* 2010, **362**, 478.

34 Y. F. Zhang, I. H. Musseman, J. P. Ferraris, K. J. Balkus, *J. Membr. Sci*. 2008, **313**, 170.
35 R. Adams, C. Carson, J. Ward, R. Tannenbaum, W. Koros, *Microporous Mesoporous Mat.* 2010, **131**, 13.
36 K. Diaz, L. Garrido, M. Lopez-Gonzalez, L. F. del Castillo, E. Riande, *Macromolecules* 2010, **43**, 316.
37 S. Basu, M. Maes, A. Cano-Odena, L. Alaerts, D. E. De Vos, I. F. J. Vankelecom, *J. Membr. Sci*. 2009, **344**, 190.
38 R. Ostermann, J. Cravillon, C. Weidmann, M. Wiebcke, B. M. Smarsly, *Chem. Commun.* 2011, **47**, 442.
39 L. L. Fan, M. Xue, Z. X. Kang, H. Li and S. L. Qiu, *J. Mater. Chem.*, 2012, **22**, 25272.
40 Y. N. Wu, F. T. Li, H. M. Liu, W. Zhu, M. M. Teng, Y. Jiang, W. N. Li, D. Xu, D. H. He, P. Hannam and G. T. Li, *J. Mater. Chem.*, 2012, **22**, 16971.
41 R. Ameloot, A. Liekens, L. Alaerts, M. Maes, A. Galarneau, B. Coq, G. Desmet, B. F. Sels, J. F. M. Denayer, D. E. De Vos, *Eur. J. Inorg. Chem*. 2010, 3735.
42 A. Ahmed, M. Forster, R. Clowes, D. Bradshaw, P. Myers, H. F. Zhang, *J. Mater. Chem. A* 2013, **1**, 3276.
43 S. Aguado, J. Canivet, D. Farrusseng, *Chem. Commun*. 2010, **46**, 7999.
44 M. L. Pinto, S. Dias, J. Pires, *ACS Appl. Mater. Interfaces* 2013, **5**, 2360.
45 D. Nagaraju, D. G. Bhagat, R. Banerjee, U. K. Kharul, *J. Mater. Chem. A* 2013, **1**, 8828.
46 L. D. O'Neill, H. F. Zhang, D. Bradshaw, *J. Mater. Chem.* 2010, **20**, 5720.
47 D. Qian, C. Lei, G. P. Hao, W. C. Li, A. H. Lu, *ACS Appl. Mater. Interfaces* 2012, **4**, 6125.
48 Y. J. Cui, Y. F. Yue, G. D. Qian, B. L. Chen, *Chem. Rev*. 2012, **112**, 1126.
49 W. J. Rieter, K. M. Pott, K. M. L. Taylor, W. B. Lin, *J. Am. Chem. Soc.* 2008, **130**, 11584.
50 D. M. Liu, R. C. Huxford, W. B. Lin, *Angew. Chem. Int. Edit.* 2011, **50**, 3696.
51 K. M. L. Taylor, W. J. Rieter, W. B. Lin, *J. Am. Chem. Soc*. 2008, **130**, 14358.
52 M. G. Schwab, I. Senkovska, M. Rose, M. Koch, J. Pahnke, G. Jonschker, S. Kaskel, *Adv. Eng. Mater.* 2008, **10**, 1151.
53 M. Sabo, A. Henschel, H. Froede, E. Klemm, S. Kaskel, *J. Mater. Chem.* 2007, **17**, 3827.
54 A. Henschel, K. Gedrich, R. Kraehnert, S. Kaskel, *Chem. Commun.* 2008, 4192.
55 Y. Y. Pan, B. Z. Yuan, Y. W. Li, D. H. He, *Chem. Commun*. 2010, **46**, 2280.
56 A. Aijaz, A. Karkamkar, Y. J. Choi, N. Tsumori, E. Ronnebro, T. Autrey, H. Shioyama, Q. Xu, *J. Am. Chem. Soc.* 2012, **134**, 13926.
57 Q. L. Zhu, J. Li, Q. Xu, *J. Am. Chem. Soc*. 2013, **135**, 10210.
58 Y. B. A. Huang, Z. L. Zheng, T. F. Liu, J. Lu, Z. J. Lin, H. F. Li, R. Cao, *Catal. Commun*. 2011, **14**, 27.
59 Y. B. Huang, S. Y. Gao, T. F. Liu, J. Lu, X. Lin, H. F. Li, R. Cao, *ChemPlusChem* 2012, **77**, 106.
60 Y. K. Hwang, D. Y. Hong, J. S. Chang, S. H. Jhung, Y. K. Seo, J. Kim, A. Vimont, M. Daturi, C. Serre, G. Ferey, A*ngew. Chem. Int. Edit.* 2008, **47**, 4144.
61 G. Ferey, C. Mellot-Draznieks, C. Serre, F. Millange, J. Dutour, S. Surble, I. Margiolaki, *Science* 2005, **309**, 2040.
62 M. Muller, A. Devaux, C. H. Yang, L. De Cola, R. A. Fischer, *Photochem. Photobiol. Sci.* 2010, **9**, 846.
63 S. Hermes, F. Schroder, S. Amirjalayer, R. Schmid, R. A. Fischer, *J. Mater. Chem.* 2006, **16**, 2464.
64 M. Muller, S. Hermes, K. Kaehler, M. W. E. van den Berg, M. Muhler, R. A. Fischer, *Chem. Mat.* 2008, **20**, 4576.
65 M. Muller, X. N. Zhang, Y. M. Wang, R. A. Fischer, *Chem. Commun.* 2009, 119.
66 D. Esken, S. Turner, C. Wiktor, S. B. Kalidindi, G. Van Tendeloo, R. A. Fischer, *J. Am. Chem. Soc*. 2011, **133**, 16370.
67 B. H. Hong, S. C. Bae, C. W. Lee, S. Jeong, K. S. Kim, *Science* 2001, **294**, 348.
68 Y. E. Cheon, M. P. Suh, *Angew. Chem. Int. Edit.* 2009, **48**, 2899.
69 Y. H. Wei, S. B. Han, D. A. Walker, P. E. Fuller, B. A. Grzybowski, *Angew. Chem. Int. Edit.* 2012, **51**, 7435.
70 H. R. Moon, J. H. Kim, M. P. Suh, *Angew. Chem. Int. Edit.* 2005, **44**, 1261.
71 M. P. Suh, H. R. Moon, E. Y. Lee, S. Y. Jang, *J. Am. Chem. Soc.* 2006, **128**, 4710.
72 Y. E. Cheon, M. P. Suh, *Chem.-Eur. J.* 2008, **14**, 3961.
73 H. R. Moon, M. P. Suh, *Eur. J. Inorg. Chem.* 2010, 3795.
74 S. Hermes, M. K. Schroter, R. Schmid, L. Khodeir, M. Muhler, A. Tissler, R. W. Fischer, R. A. Fischer, *Angew. Chem. Int. Edit.* 2005, **44**, 6237.
75 F. Schroeder, D. Esken, M. Cokoja, M. W. E. van den Berg, O. I. Lebedev, G. van Tendeloo, B. Walaszek, G. Buntkowsky, H. H. Limbach, B. Chaudret, R. A. Fischer, *J. Am. Chem. Soc*. 2008, **130**, 6119.
76 D. Esken, S. Turner, O. I. Lebedev, G. Van Tendeloo, R. A. Fischer, *Chem. Mat.* 2010, **22**, 6393.
77 Y. K. Park, S. B. Choi, H. J. Nam, D. Y. Jung, H. C. Ahn, K. Choi, H. Furukawa, J. Kim, *Chem. Commun.* 2010, **46**, 3086.
78 J. Juan-Alcaniz, E. V. Ramos-Fernandez, U. Lafont, J. Gascon and F. Kapteijn, *J. Catal.*, 2010, **269**, 229.
79 S. X. Gao, N. Zhao, M. H. Shu, S. N. Che, *Appl. Catal. A-Gen.* 2010, **388**, 196.
80 T. T. Dang, Y. H. Zhu, S. C. Ghosh, A. Q. Chen, C. L. L. Chai, A. M. Seayad, *Chem. Commun.* 2012, **48**, 1805.
81 H. L. Jiang, T. Akita, T. Ishida, M. Haruta, Q. Xu, *J. Am. Chem. Soc.* 2011, **133**, 1304.
82 H. L. Liu, Y. L. Liu, Y. W. Li, Z. Y. Tang, H. F. Jiang, *J. Phys. Chem. C* 2010, **114**, 13362.
83 M. S. El-Shall, V. Abdelsayed, A. Khder, H. M. A. Hassan, H. M. El-Kaderi, T. E. Reich, *J. Mater. Chem.* 2009, **19**, 7625.
84 F. Wu, L. G. Qiu, F. Ke, X. Jiang, *Inorg. Chem. Commun*. 2013, **32**, 5.
85 H. L. Liu, Y. W. Li, R. Luque, H. F. Jiang, *Adv. Synth. Catal.* 2011, **353**, 3107.
86 B. Z. Yuan, Y. Y. Pan, Y. W. Li, B. L. Yin, H. F. Jiang, *Angew. Chem. Int. Edit.* 2010, **49**, 4054.
87 Y. B. Huang, Z. J. Lin, R. Cao, *Chem.-Eur. J.* 2011, **17**, 12706.
88 H. Zhang, M. S. Jin, Y. N. Xia, *Chem. Soc. Rev.* 2012, **41**, 8035.
89 N. S. Porter, H. Wu, Z. W. Quan, J. Y. Fang, *Accounts Chem. Res.* 2013, **46**, 1867.

90 B. Z. Zhan, X. Y. Li, *Chem. Commun.* 1998, 349.
91 C. Y. Sun, S. X. Liu, D. D. Liang, K. Z. Shao, Y. H. Ren, Z. M. Su, *J. Am. Chem. Soc.* 2009, **131**, 1883.
92 J. Juan-Alcaniz, E. V. Ramos-Fernandez, U. Lafont, J. Gascon, F. Kapteijn, *J. Catal.* 2010, **269**, 229.
93 R. Canioni, C. Roch-Marchal, F. Secheresse, P. Horcajada, C. Serre, M. Hardi-Dan, G. Ferey, J. M. Greneche, F. Lefebvre, J. S. Chang, Y. K. Hwang, O. Lebedev, S. Turner, G. Van Tendeloo, *J. Mater. Chem.* 2011, **21**, 1226.
94 T. Tsuruoka, H. Kawasaki, H. Nawafune, K. Akamatsu, *ACS Appl. Mater. Interfaces* 2011, **3**, 3788.
95 F. Wang, R. Deng, J. Wang, Q. Wang, Y. Han, H. Zhu, X. Chen, X. Liu. *Nat. Mater.*, 2011, **10**, 968.
96 F. Ke, J. F. Zhu, L. G. Qiu, X. Jiang, *Chem. Commun.* 2013, **49**, 1267.
97 P. Wang, J. Zhao, X. B. Li, Y. Yang, Q. H. Yang, C. Li, *Chem. Commun.* 2013, **49**, 3330.
98 M. R. Lohe, K. Gedrich, T. Freudenberg, E. Kockrick, T. Dellmann, S. Kaskel, *Chem. Commun.* 2011, **47**, 3075.
99 G. Lu, S. Z. Li, Z. Guo, O. K. Farha, B. G. Hauser, X. Y. Qi, Y. Wang, X. Wang, S. Y. Han, X. G. Liu, J. S. DuChene, H. Zhang, Q. C. Zhang, X. D. Chen, J. Ma, S. C. J. Loo, W. D. Wei, Y. H. Yang, J. T. Hupp, F. W. Huo, *Nat. Chem.* 2012, **4**, 310.
100 S. Z. Li, F. W. Huo. *Small* 2014, **10**, 4371.
101 C. H. Kuo, Y. Tang, L. Y. Chou, B. T. Sneed, C. N. Brodsky, Z. P. Zhao, C. K. Tsung, *J. Am. Chem. Soc.* 2012, **134**, 14345.
102 S. Furukawa, K. Hirai, K. Nakagawa, Y. Takashima, R. Matsuda, T. Tsuruoka, M. Kondo, R. Haruki, D. Tanaka, H. Sakamoto, S. Shimomura, O. Sakata, S. Kitagawa, *Angew. Chem. Int. Edit.* 2009, **48**, 1766.
103 S. Furukawa, K. Hirai, Y. Takashima, K. Nakagawa, M. Kondo, T. Tsuruoka, O. Sakata, S. Kitagawa, *Chem. Commun*. 2009, 5097.
104 K. Hirai, S. Furukawa, M. Kondo, H. Uehara, O. Sakata, S. Kitagawa, *Angew. Chem. Int. Edit.* 2011, **50**, 8057.
105 K. Koh, A. G. Wong-Foy, A. J. Matzger, *Chem. Commun.* 2009, 6162.
106 T. Li, J. E. Sullivan, N. L. Rosi, *J. Am. Chem. Soc.* 2013, **135**, 9984.
107 J. Reboul, S. Furukawa, N. Horike, M. Tsotsalas, K. Hirai, H. Uehara, M. Kondo, N. Louvain, O. Sakata, S. Kitagawa, *Nat. Mater.* 2012, **11**, 717.
108 J. R. Kira Khaletskaya, Mikhail MeilikhovMasashi Nakahama, Stephane Diring, S. I. Masahiko Tsujimoto, Franklin Kim, Ken-ichiro Kamei, Roland A. Fischer. S. F. Susumu Kitagawa, *J. Am. Chem. Soc*. 2013, **135**, 8.
109 W. W. Zhan, Q. Kuang, J. Z. Zhou, X. J. Kong, Z. X. Xie, L. S. Zheng, *J. Am. Chem. Soc.* 2013, **135**, 1926.
110 S. Z. Li, W. Zhang, Y. Liu, Q.Zhao, F. W. Huo. *Cryst. Grow & Des.* 2015, DOI: 10.1021/cg501551y.
111 Y. Y. Liu, W. N. Zhang, S. Z. Li, C. L. Cui, J. Wu, H. Y. Chen, F. W. Huo, *Chem. Mat.* 2014, **26**, 1119.
112 R. G. Chaudhuri, S. Paria, *Chem. Rev.* 2012, **112**, 2373.
113 L. C. He, Y. Liu, J. Z. Liu, Y. S. Xiong, J. Z. Zheng, Y. L. Liu, Z. Y. Tang, *Angew. Chem. Int. Edit.* 2013, **52**, 3741.
114 C. Petit, J. Burress, T. J. Bandosz, *Carbon* 2011, **49**, 563.
115 C. Petit, T. J. Bandosz, *Adv. Funct. Mater.* 2011, **21**, 2108.
116 C. Petit, T. J. Bandosz, *Adv. Mater.* 2009, **21**, 4753.
117 C. Petit, T. J. Bandosz, *Adv. Funct. Mater.* 2010, **20**, 111.
118 M. Jahan, Q. L. Bao, K. P. Loh, *J. Am. Chem. Soc.* 2012, **134**, 6707.
119 T. Ishida, M. Nagaoka, T. Akita, M. Haruta, *Chem.-Eur. J.* 2008, **14**, 8456.
120 H. L. Jiang, B. Liu, T. Akita, M. Haruta, H. Sakurai, Q. Xu, *J. Am. Chem. Soc.* 2009, **131**, 11302.
121 H. L. Jiang, Q. P. Lin, T. Akita, B. Liu, H. Ohashi, H. Oji, T. Honma, T. Takei, M. Haruta, Q. Xu, *Chem.-Eur. J.* 2011, **17**, 78.
122 P. Marc. *Chem. Rev*., 2014, **114**, 1413.
123 C. Petit, T. J. Bandosz. *J. Colloid Interface Sci.* doi: 10.1016/j.jcis.2014.08.026.
124 R. Kumar, K. Jayaramulu, T. K. Maji, C. N. R. Rao, *Chem. Commun.* 2013, **49**, 4947.
125 Y. X. Zhao, M. Seredych, Q. Zhong, T. J. Bandosz, *ACS Appl. Mater. Interfaces* 2013, **5**, 4951.
126 C. Petit, T. J. Bandosz, *Dalton Trans.* 2012, **41**, 4027.
127 C. Petit, B. Mendoza, T. J. Bandosz, *ChemPhysChem* 2010, **11**, 3678.
128 C. Petit, B. Levasseur, B. Mendoza, T. J. Bandosz, *Microporous Mesoporous Mat.* 2012, **154**, 107.
129 M. M. K. Salem, P. Braeuer, M. von Szombathely, M. Heuchel, P. Harting, K. Quitzsch, M. Jaroniec, *Langmuir* 1998, **14**, 3376.
130 O. K. Farha, A. O. Yazaydin, I. Eryazici, C. D. Malliakas, B. G. Hauser, M. G. Kanatzidis, S. T. Nguyen, R. Q. Snurr, J. T. Hupp, *Nat. Chem*. 2010, **2**, 944-948.
131 H. Furukawa, N. Ko, Y. B. Go, N. Aratani, S. B. Choi, E. Choi, A. O. Yazaydin, R. Q. Snurr, M. O'Keeffe, J. Kim, O. M. Yaghi, *Science* 2010, **329**, 424.
132 K. M. Thomas, *Catal. Today* 2007, **120**, 389.
133 J. X. Dong, X. Y. Wang, H. Xu, Q. Zhao, J. P. Li, *Int. J. Hydrog. Energy* 2007, **32**, 4998.
134 S. J. Yang, J. Y. Choi, H. K. Chae, J. H. Cho, K. S. Nahm, C. R. Park, *Chem. Mat.* 2009, **21**, 1893.
135 K. P. Prasanth, P. Rallapalli, M. C. Raj, H. C. Bajaj, R. V. Jasra, *Int. J. Hydrog. Energy* 2011, **36**, 7594.
136 S. Liu, L. X. Sun, F. Xu, J. Zhang, C. L. Jiao, F. Li, Z. B. Li, S. Wang, Z. Q. Wang, X. Jiang, H. Y. Zhou, L. N. Yang, C. Schick, *Energy Environ. Sci.* 2013, **6**, 818.
137 Y. W. Li, R. T. Yang, *J. Am. Chem. Soc.* 2006, **128**, 8136.
138 C. S. Tsao, M. S. Yu, C. Y. Wang, P. Y. Liao, H. L. Chen, U. S. Jeng, Y. R. Tzeng, T. Y. Chung, H. C. Wut, *J. Am. Chem. Soc.* 2009, **131**, 1404.
139 M. A. Miller, C. Y. Wang, G. N. Merrill, *J. Phys. Chem. C* 2009, **113**, 3222.
140 N. R. Stuckert, L. F. Wang, R. T. Yang, *Langmuir* 2010, **26**, 11963.
141 M. Anbia, S. Mandegarzad, *J. Alloy. Compd.* 2012, **532**, 61.
142 Y. Y. Liu, J. Zhang, J. L. Zeng, H. L. Chu, F. Xu, L. X. Sun, *Chin. J. Catal.* 2008, **29**, 655.
143 S. Proch, J. Herrmannsdorfer, R. Kempe, C. Kern, A. Jess, L. Seyfarth, J. Senker, *Chem.-Eur. J.* 2008, **14**, 8204.
144 C. Zlotea, R. Campesi, F. Cuevas, E. Leroy, P. Dibandjo, C. Volkringer, T. Loiseau, G. Ferey, M. Latroche, *J. Am. Chem. Soc.* 2010, **132**, 2991.
145 N. A. Khan, S. H. Jhung. *Angrew. Chem. Int. Edit.*, 2012, **51**, 1198.
146 N. A. Khan, S. H. Jhung. *J. Hazard. Mater.*, 2012, **237**, 180.
147 I. Ahmed, S. H. Jhung. *Chem. Eng. J.*, 2014, **251**, 35.
148 I. Ahmed, N. A. Khan, Z. Hasan, S. H. Jhung. *J. Hazard. Mater.*, 2013, **250**, 37.

149 N. A. Khan, S. H. Jhung. *Fuel Process. Technol*., 2012, **100**, 49.
150 I. Ahmed, N. A. Khan, S. H. Jhung. *Inorg. Chem.*, 2013, **52**, 14155.
151 G. G. Chang, Z. B. Bao, Q. L. Ren, S. G. Deng, Z. G. Zhang, B. G. Su, H. B. Xing, Y. W. Yang. *RSC Adv.*, 2014, **4**, 20230.
152 W. P. Qin, W. X. Cao, H. L. Liu, Z. Li, Y. W. Li. *RSC Adv.*, 2014, **4**, 2414.
153 B. Seoane, C. Tellez, J. Coronas, C. Staudt, *Sep. Purif. Technol.* 2013, **111**, 72.
154 T. Li, Y. C. Pan, K. V. Peinemann, Z. P. Lai, *J. Membr. Sci.* 2013, **425**, 235.
155 J. G. Won, J. S. Seo, J. H. Kim, H. S. Kim, Y. S. Kang, S. J. Kim, Y. M. Kim, J. G. Jegal, *Adv. Mater*. 2005, **17**, 80.
156 B. Zornoza, A. Martinez-Joaristi, P. Serra-Crespo, C. Tellez, J. Coronas, J. Gascon, F. Kapteijn, *Chem. Commun*. 2011, **47**, 9522.
157 H. B. T. Jeazet, C. Staudt, C. Janiak, *Chem. Commun.* 2012, **48**, 2140.
158 L. Ge, W. Zhou, V. Rudolph, Z. H. Zhu, *J. Mater. Chem. A* 2013, **1**, 6350.
159 S. N. Wijenayake, N. P. Panapitiya, S. H. Versteeg, C. N. Nguyen, S. Goel, K. J. Balkus, I. H. Musselman, J. P. Ferraris, *Ind. Eng. Chem. Res.* 2013, **52**, 6991.
160 X. Y. Chen, H. Vinh-Thang, D. Rodrigue, S. Kaliaguine, *Ind. Eng. Chem. Res*. 2012, **51**, 6895.
161 J. Hu, H. P. Cai, H. Q. Ren, Y. M. Wei, Z. L. Xu, H. L. Liu, Y. Hu, *Ind. Eng. Chem. Res*. 2010, **49**, 12605.
162 P. G. Sara Sorribas, Carlos Téllez, Joaquín Coronas, and Andrew G. Livingston, *J. Am. Chem. Soc*. 2013, **135**, 8.
163 Y. Y. Fu, C. X. Yang, X. P. Yan, *Chem.-Eur. J.* 2013, **19**, 13484.
164 A. Dhakshinamoorthy, H. Garcia, *Chem. Soc. Rev*. 2012, **41**, 5262.
165 C. L. Hill, C. M. Prossermccartha, *Coord. Chem. Rev.* 1995, **143**, 407.
166 K. Inumaru, T. Ishihara, Y. Kamiya, T. Okuhara, S. Yamanaka, *Angew. Chem. Int. Edit.* 2007, **46**, 7625.
167 H. Yang, J. Li, L. Y. Wang, W. Dai, Y. Lv, S. Gao, *Catal. Commun.* 2013, **35**, 101.
168 L. H. Wee, S. R. Bajpe, N. Janssens, I. Hermans, K. Houthoofd, C. E. A. Kirschhock, J. A. Martens, *Chem. Commun*. 2010, **46**, 8186.
169 D. D. Liang, S. X. Liu, F. J. Ma, F. Wei, Y. G. Chen, *Adv. Synth. Catal.* 2011, **353**, 733.
170 B. Xiao, P. S. Wheatley, X. B. Zhao, A. J. Fletcher, S. Fox, A. G. Rossi, I. L. Megson, S. Bordiga, L. Regli, K. M. Thomas, R. E. Morris, *J. Am. Chem. Soc*. 2007, **129**, 1203.
171 Y. M. Zhang, V. Degirmenci, C. Li, E. J. M. Hensen, *ChemSusChem* 2011, **4**, 59.
172 C. G. Silva, I. Luz, F. Xamena, A. Corma, H. Garcia, *Chem.-Eur. J.* 2010, **16**, 11133.
173 Y. H. Fu, D. R. Sun, Y. J. Chen, R. K. Huang, Z. X. Ding, X. Z. Fu, Z. H. Li, *Angew. Chem. Int. Edit.* 2012, **51**, 3364.
174 Y. Kataoka, Y. Miyazaki, K. Sato, T. Saito, Y. Nakanishi, Y. Kiatagwa, T. Kawakami, M. Okumura, K. Yamaguchi, W. Mori, *Supramol. Chem.* 2011, **23**, 287.
175 S. Y. Jin, H. J. Son, O. K. Farha, G. P. Wiederrecht, J. T. Hupp, *J. Am. Chem. Soc.* 2013, **135**, 955.
176 J. He, Z. Y. Yan, J. Q. Wang, J. Xie, L. Jiang, Y. M. Shi, F. G. Yuan, F. Yu, Y. J. Sun, *Chem. Commun*. 2013, **49**, 6761.
177 J. Della Rocca, D. M. Liu, W. B. Lin, *Accounts Chem. Res.* 2011, **44**, 957.
178 W. J. Rieter, K. M. L. Taylor, W. B. Lin, *J. Am. Chem. Soc.* 2007, **129**, 9852.
179 M. D. Rowe, D. H. Thamm, S. L. Kraft, S. G. Boyes, *Biomacromolecules* 2009, **10**, 983.
180 K. M. L. Taylor-Pashow, J. Della Rocca, Z. G. Xie, S. Tran, W. B. Lin, *J. Am. Chem. Soc*. 2009, **131**, 14261.
181 Y. W. Jun, J. W. Seo, A. Cheon, *Accounts Chem. Res.* 2008, **41**, 179.
182 R. Hergt, S. Dutz, M. Roder, J. *Phys.-Condes. Matter* 2008, 20.
183 S. Eustis, M. A. El-Sayed, *Chem. Soc. Rev.* 2006, **35**, 209.
184 D. M. D'Alessandro, J. R. R. Kanga, J. S. Caddy, *Aust. J. Chem.* 2011, **64**, 718.
185 Y. Kobayashi, B. Jacobs, M. D. Allendorf, J. R. Long, *Chem. Mat.* 2010, **22**, 4120.
186 H. Miyasaka, *Accounts Chem. Res.* 2013, **46**, 248.
187 D. Umeyama, S. Horike, M. Inukai, Y. Hijikata, S. Kitagawa, *Angew. Chem. Int. Edit.* 2011, **50**, 11706.
188 S. Bureekaew, S. Horike, M. Higuchi, M. Mizuno, T. Kawamura, D. Tanaka, N. Yanai, S. Kitagawa, *Nat. Mater*. 2009, **8**, 831.
189 M. Sadakiyo, T. Yamada, H. Kitagawa, *J. Am. Chem. Soc*. 2009, **131**, 9906.
190 M. Yoon, K. Suh, S. Natarajan, K. Kim, *Angew. Chem. Int. Edit.* 2013, **52**, 2688.
191 H. A. Becerril, J. Mao, Z. Liu, R. M. Stoltenberg, Z. Bao, Y. Chen, *ACS Nano* 2008, **2**, 463.
192 Z. L. Maryam Jahan, Kian Ping Loh, *Adv. Funct. Mater*. 2013, **23**, 5363.
193 M. L. Pang, A. J. Cairns, Y. L. Liu, Y. Belmabkhout, H. C. Zeng, M. Eddaoudi, *J. Am. Chem. Soc*. 2012, **134**, 13176.
194 C. E. Wilmer, O. K. Farha, Y. S. Bae, J. T. Hupp, R. Q. Snurr, *Energy Environ. Sci.* 2012, **5**, 9849.
195 C. Serre, C. Mellot-Draznieks, S. Surble, N. Audebrand, Y. Filinchuk, G. Ferey, *Science* 2007, **315**, 1828.
196 R. B. Getman, Y. S. Bae, C. E. Wilmer, R. Q. Snurr, *Chem. Rev.* 2012, **112**, 703.
197 C. R. Henry, *Surf. Sci. Rep.* 1998, **31**, 235.